

Salinity changes in the World Ocean since 1950 in relation to changing surface freshwater fluxes

Nikolaos Skliris · Robert Marsh · Simon A. Josey ·
Simon A. Good · Chunlei Liu · Richard P. Allan

Received: 28 March 2013 / Accepted: 28 March 2014 / Published online: 9 April 2014
© Springer-Verlag Berlin Heidelberg 2014

Abstract Global hydrographic and air–sea freshwater flux datasets are used to investigate ocean salinity changes over 1950–2010 in relation to surface freshwater flux. On multi-decadal timescales, surface salinity increases (decreases) in evaporation (precipitation) dominated regions, the Atlantic–Pacific salinity contrast increases, and the upper thermocline salinity maximum increases while the salinity minimum of intermediate waters decreases. Potential trends in E–P are examined for 1950–2010 (using two reanalyses) and 1979–2010 (using four reanalyses and two blended products). Large differences in the 1950–2010 E–P trend patterns are evident in several regions, particularly the North Atlantic. For 1979–2010 some coherency in the spatial change patterns is evident but there is still a large spread in trend magnitude and sign between the six E–P products. However, a robust pattern of increased E–P in the southern hemisphere subtropical gyres is seen in all products. There is also some evidence in the tropical Pacific for a link between the spatial change patterns of

salinity and E–P associated with ENSO. The water cycle amplification rate over specific regions is subsequently inferred from the observed 3-D salinity change field using a salt conservation equation in variable isopycnal volumes, implicitly accounting for the migration of isopycnal surfaces. Inferred global changes of E–P over 1950–2010 amount to an increase of $1 \pm 0.6 \%$ in net evaporation across the subtropics and an increase of $4.2 \pm 2 \%$ in net precipitation across subpolar latitudes. Amplification rates are approximately doubled over 1979–2010, consistent with accelerated broad-scale warming but also coincident with much improved salinity sampling over the latter period.

Keywords Salinity · Freshwater flux · Evaporation · Precipitation · Hydrological cycle

1 Introduction

The global water cycle, a key component of the climate system, is expected to intensify with anthropogenic global warming (Held and Soden 2006; Solomon et al. 2007). The Clausius–Clapeyron relationship indicates increases in moisture and its horizontal transport in the lower troposphere as a response to warming. Increased atmospheric moisture tends to strengthen the global Evaporation (E) minus Precipitation (P) pattern, with wet regions becoming wetter and dry regions becoming drier (Held and Soden 2006). The IPCC report on Climate Change and Water (2008) highlighted the increasingly compelling evidence over the last 50 years that the hydrological cycle has already changed. Observations show precipitation increasing in the high-latitudes and moist regions of the tropical circulation, and decreasing in dry subtropical

N. Skliris (✉) · R. Marsh
Ocean and Earth Science, National Oceanography Centre,
Southampton, University of Southampton, European Way,
Southampton SO14 3ZH, UK
e-mail: N.Skliris@noc.soton.ac.uk

S. A. Josey
National Oceanography Centre, European Way,
Southampton SO14 3ZH, UK

S. A. Good
Met Office Hadley Centre, FitzRoy Road, Exeter,
Devon EX1 3PB, UK

C. Liu · R. P. Allan
National Centre for Atmospheric Science, University of
Reading, Reading, Berkshire, UK

regions (Zhang et al. 2007; Wentz et al. 2007; Allan et al. 2010; Li et al. 2011).

Since regional salinity variations are mainly determined by variations in the air–sea freshwater budget (Schmitt 2008), the salinity field is an integrator for changes in the water cycle over the ocean, which receives over 80 % of the total global rainfall (Trenberth et al. 2007; Schanze et al. 2010). The spatial pattern of global ocean surface salinity change since 1950 provides strong evidence for an amplified water cycle (Durack et al. 2012). Large and spatially coherent multi-decadal increasing (decreasing) salinity trends have been reported in evaporation (precipitation) dominated regions (Antonov et al. 2002; Curry et al. 2003; Boyer et al. 2005; Bindoff et al. 2007; Cravatte et al. 2009; Hosoda et al. 2009; Helm et al. 2010; Durack and Wijffels 2010; Delcroix et al. 2011). Moreover, a pronounced accentuation of the salinity contrast is observed between Atlantic and Pacific Oceans throughout the upper water column, as well as between the upper thermocline salinity maximum and the salinity minimum intermediate waters within both ocean basins (Helm et al. 2010; Durack and Wijffels 2010). Recent studies of detection and attribution of anthropogenic climate change showed that the strong salinification of the subtropical North Atlantic and freshening of the Western Pacific Warm Pool over recent decades significantly exceeded the range of internal natural variability in control simulations of coupled climate models, revealing a possible early fingerprint of anthropogenic forcing (Stott et al. 2008; Terray et al. 2012; Pierce et al. 2012). These spatial patterns of observed surface salinity change are consistent with studies on atmospheric components of the water cycle such as precipitation (Wentz et al. 2007; Zhang et al. 2007; Allan et al. 2010; Li et al. 2011), column integrated water vapour (Santer et al. 2007; Li et al. 2011), and surface humidity (Willett et al. 2007).

Long-term changes in global ocean E and P may be assessed from historical climate model simulations and Numerical Weather Prediction (NWP) model reanalyses constrained by assimilated observational products such as SST and surface meteorological parameters. However, General Circulation Models (GCMs) show very large variations concerning projected changes in P and E (Meehl et al. 2007) whilst they appear to underestimate the P, E and surface salinity response to surface warming compared with observations (Wentz et al. 2007; Durack et al. 2012, Liu et al. 2012). Furthermore, estimates of 50-year trends in both freshwater flux and surface salinity derived from Coupled Model Intercomparison Project phase 3 (CMIP3) historical simulations present a very large spread among the various model outputs (e.g. Durack et al. 2012).

Major issues are also reported when estimating variability and trends in hydrological cycle components and surface freshwater fluxes from re-analysis products.

Trenberth et al. (2005) found major problems in the means, variability and trends in precipitable water over the ocean from 1988 to 2001 for both the ERA-40 and NCEP re-analysis products, highlighting the need for data re-processing and for taking into account of the changing observing system as improved temperature and water vapour channels were assimilated. Trenberth and Smith (2005) also indicated that both the above re-analysis products violate the conservation of dry air–mass and present substantial spurious changes in surface pressures due to water vapour prior to the start of the satellite era in 1979. Schanze et al. (2010) investigated seven objectively-analyzed and re-analyzed P and E datasets and showed relatively large differences in the estimates of global annual surface freshwater balances. The authors identified inhomogeneities in all these E and P products before 1987 which they mainly attributed to the inclusion of Special Sensor Microwave Imager (SSM/I) data thereafter. More recently, Trenberth et al. (2011) assessed the global hydrological cycle and its variability from eight re-analysis products. The authors reported significant differences in estimates of E–P change over the ocean among most re-analysis products. In addition the authors found that re-analysis output data violate basic physical constraints and often are inconsistent with observational estimates, with most of the re-analysis models showing too-intense water cycling overestimating P and E.

Due to the highly sporadic and localised character of rainfall, and the large difficulties in obtaining reliable in situ measurements of P and E over the ocean, there is a very high level of uncertainty in the estimation of observed ocean surface freshwater fluxes. Before the advent of operational satellite observation, the estimation of surface freshwater fluxes was based on indirect ship-borne precipitation estimates that made use of the reported weather conditions. Consequently large oceanic regions (the Southern Ocean, in particular) were considerably under-sampled. Global ocean precipitation observational datasets such as the Global Precipitation Climatology Project (GPCP) and CPC's Merged Analysis of Precipitation (CMAP) datasets are available since the start of the satellite era in 1979 based on precipitation estimates from several satellite-based retrievals and ground-based rain gauges. The Hamburg Ocean–Atmosphere Parameters and Fluxes from Satellite Data version 3 (HOAPS3) dataset, the first satellite-based dataset with consistently derived global fields of both E and P only starts in 1987 (Andersson et al. 2011). Although there is more agreement among the satellite-derived products, as compared with in situ and reanalysis products, the uncertainty in estimating precipitation is still high (Wentz et al. 2007; Lau and Wu 2007; Tian et al. 2009; Schanze et al. 2010; Arkin et al. 2010), with the various global ocean precipitation products

showing rather large variations (e.g. Yin et al. 2004; Andersson et al. 2011; Liu and Allan 2012). Despite the fact that most of the data sources used are generally common, different merging algorithms and choices of including/excluding or blending data are shown to produce substantial discrepancies in the precipitation patterns over the ocean among the global observational datasets (e.g. Yin et al. 2004). Substantial spatial and temporal discrepancies are also found among the various re-analysis/objectively-analysed latent heat flux products which can be attributed to the use of different sources of the input meteorological state variables and bulk formulae (e.g. Liu et al. 2011). Direct E–P estimates are still very sparse and despite the abovementioned large problems encountered when estimating long-term trends using re-analyses or combined re-analysis/satellite-derived observational products, the latter provide our only insights into the changing global E–P field through time.

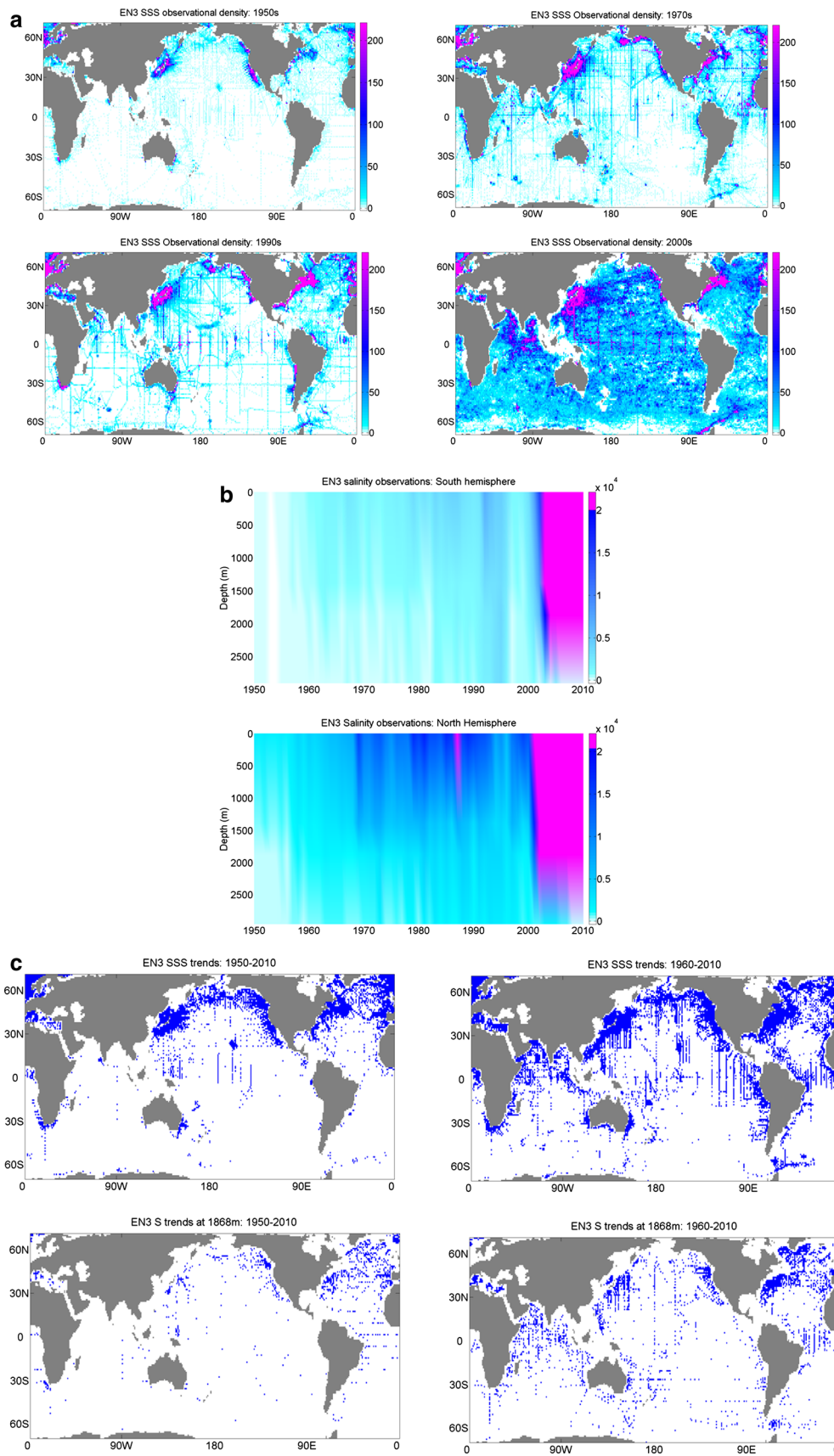
Similarly to freshwater flux measurements, historic salinity measurements in the southern hemisphere, and in particular in the Southern Ocean, remained extremely sparse until the late 1980s, limiting accuracy in estimates of global change. However, the World Ocean Circulation Experiment (WOCE, 1988–1996) and the ARGO network after 1999 have crucially enhanced southern hemisphere coverage, substantially improving analyses of long-term variability at global scale. Durack et al. (2012) suggested that the common findings of independent studies that considered salinity changes, along with the strong E–P versus surface salinity relationship in CMIP3 models, underpin salinity as a very useful marker of long-term global water cycle change. However, the 3-D pattern of salinity change is very complex as it is shaped by advection and mixing at the timescales on which salinity anomalies are spreading through the ocean interior. Salinity anomalies induced by surface freshwater flux anomalies are generally subducted from the surface to sub-surface layers within the main thermocline following isopycnal surfaces. Since diapycnal mixing is generally weak, salinity anomalies transported from their surface formation sites into the ocean interior along isopycnal surfaces can be largely preserved so that surface freshwater fluxes may potentially be inferred from these sub-surface salinity changes (Bindoff and McDougall 1994; Helm et al. 2010). However, sub-surface salinity changes in the global ocean may also occur with a locally invariant air-sea freshwater budget. Such changes may be induced by the horizontal shift in isopycnal outcrops that is predominantly poleward in the case of broad-scale warming (Durack and Wijffels 2010), as well as by changes in the hydrographic properties of overflows from marginal seas such as the Mediterranean outflow in the North Atlantic (e.g. Curry et al. 2003; Potter and Lozier 2004).

The overall objective of this paper is to provide new insights into the link between global ocean salinity changes and the surface freshwater flux anomalies associated with the changing water cycle over the last 60 years using a range of observational/reanalysis datasets. In particular we investigate the spatial correlation patterns of E–P and surface salinity time series, and the propagation pathways and timescales of salinity anomalies from their surface formation sites into the ocean interior. The analysis is also performed for the shorter 1979–2010 period covering the satellite era, where both reconstructed global E–P and surface salinity fields are better constrained by available data, allowing for a more accurate representation of their co-variability at inter-annual/inter-decadal scales. Moreover, we use a methodology based on salt conservation equation in volumes bounded by space/time variable isopycnal surfaces, following the migration of isopycnal surface outcrops to infer changes in the air-sea freshwater fluxes from the observed salinity changes in each oceanic basin.

This paper is organized as follows. First, we introduce the salinity and freshwater flux datasets. We then analyse long-term trends in these respective fields, and investigate links using correlation patterns. Given the salinity changes, we infer freshwater flux changes and subsequently we provide estimates of the water cycle amplification in various oceanic regions over 1950–2010. Finally, we conclude with a summary of our findings, emphasising caveats due to the limitations of sampling in space and time.

2 Datasets

The investigation of multi-decadal global salinity changes over 1950–2010 is performed using the UK Met Office EN3v2a observational dataset (<http://www.metoffice.gov.uk/hadobs/en3>), an update of the EN2 dataset described in Ingleby and Huddleston (2007). EN3v2a consists of quality-controlled temperature and salinity (PSS-78) profiles spanning the period 1950–present. The original sources of the profiles include the World Ocean Database (2005), the Global Temperature-Salinity Profile Programme (from 1990) and profiling float data from the Argo Global Data Assembly Center (from 1999). Observational coverage of salinity data strongly changes over the 1950–2010 period for both the near surface (Fig. 1a) and the deep layers. There is a relatively sparse coverage in the early decades of the EN3 dataset, particularly in the southern hemisphere and at depths greater than 1,000 m, improving to almost global coverage from surface to 2,000 m depth after the introduction of the Argo floats. This is illustrated in Fig. 1b, which shows the evolution of the number of salinity observations used in the EN3 dataset versus time



◀ **Fig. 1** Salinity observations used in the EN3 dataset **a** number of near-surface observations over 1950s, 1970s, 1990s, and 2000s. **b** Number of observations versus depth (0–3 000 m) and time (1950–2010) in the south and north hemispheres, respectively. **c** Grid points with sufficient number of data to determine trends over 1950–2010 (*left panels*) and over 1960–2010 (*right panels*), for near-surface salinity (*upper panels*) and for salinity at 1,868 m (*lower panels*), where the criteria for trend detection are at least five observations near-surface and at least two observations at depth, for both the starting and last decades of the record

and depth in the northern and southern hemispheres, respectively. The product used here is a monthly objectively-analysed version of the data with $1^\circ \times 1^\circ$ horizontal resolution and 42 vertical levels over the global ocean. The quality of the objective analysis clearly varies spatially depending on the availability of input data to which it is constrained. Hence observational coverage strongly limits the representation of long-term variability and trends in the deep layers and in large oceanic regions of the south hemisphere, in particular the Southern Ocean, which is poorly sampled over the 1950s and 1960s. There are consequences for trend analysis (Fig. 1c). The actual observations available for analysing 50- or 60-year trends are largely limited to the periphery of the northern oceans, a problem exacerbated at depth. We emphasise this caveat throughout our analysis. We should also note that what we term Sea Surface Salinity (SSS) in this study should actually be referred to as near-surface salinity since the EN3 upper vertical level is located at 5 m depth.

Various reanalyses/observational global ocean E–P datasets are included in the analysis and compared with the salinity dataset, covering the whole or part of the 1950–2010 period. Four reanalysis E–P products are considered here: the NCEP/NCAR Reanalysis 1 spanning 1948–present (Kistler et al. 2001); NCEP/DOE, spanning 1979–present (Kanamitsu et al. 2002); twentieth century reanalysis (20CRv2), spanning 1871–present (Compo et al. 2011); ERA-Interim, spanning 1979–present (Dee et al. 2011).

Apart from re-analysis products, a variety of combined re-analysis E and observational P global ocean products may be derived for the satellite era starting in 1979. Two products are included in the present analysis: (a) the Common Ocean-ice Reference Experiments 2 (COREv2) E–P dataset (Large and Yeager 2009) spanning the period 1979–2006, for which the E field is based on NCEP reanalyses and the P field is a blend of precipitation products including the Global Precipitation Climatology Project (GPCP) Version 2 (GPCP v2.2, Adler et al. 2003; Huffman et al. 2009) and the CPC Merged Analysis of Precipitation (CMAP) (Xie and Arkin 1996) datasets, both based on rain gauge observations over land and satellite retrievals (predominantly over ocean regions); (b) a combined product

for the period 1979–2010 for which the E field is derived by the Objectively Analyzed air–sea Fluxes (OAF flux) dataset (Yu and Weller 2007) which blends NCEP and ERA-40 reanalysis products with satellite surface meteorology through an objective synthesis, and the P field is obtained from GPCP.

More recent satellite-derived precipitation and evaporation data sources such as the Tropical Rainfall Measuring Mission (TRMM), although they are able to provide data of higher spatiotemporal coverage using radar instruments, are considered only for evaluation purposes and not used in our global ocean multi-decadal analysis due to their short record length (i.e. they are only available since 1997) and to their restricted latitudinal coverage (i.e. maximum coverage of 40°S – 40°N). The HOAPS satellite-based dataset for both E and P is also not considered here due to its short record length (i.e. 1987–2005) and contrasting variability over the ocean compared with other datasets (Liu and Allan 2012). HOAPS also shows a much higher global water cycle amplification rate with respect to other datasets (Durack et al. 2012).

3 Results and discussion

When estimating long-term climatic trends, one needs to take into account natural climate variability signals, which may have significant impacts on ocean surface variables such as salinity and freshwater fluxes at regional or even global scales. It is generally difficult to discriminate between the regional patterns of global climate change and the anomalies induced by natural low-frequency modes of large-scale atmospheric variability. In particular, pronounced intra-decadal natural variability events associated with the El Niño Southern Oscillation (ENSO) are imprinted in the spatial patterns of all water cycle variables. Moreover, there are also significant multi-decadal signals associated with low frequency expressions of modes of natural atmospheric variability that may strongly control air–sea interaction. A typical example is that of the North Atlantic Oscillation (NAO) variations over recent decades that have been shown to have large impacts on the freshwater budget and ocean circulation of the North Atlantic (Hurrell 1995; Curry and McCartney 2001). The winter NAO index underwent a large quasi-continuous increase from a negative to a highly positive phase from late 1960s to early 1990s and then abruptly decreased to a negative phase (Hurrell and Deser 2010).

Such multi-decadal signals with periods of the order of 2–3 decades may be also observed in other natural variability modes such as the Pacific Decadal Oscillation (PDO) and Atlantic Multi-decadal Oscillation (AMO) skewing long-term human-induced trends in the water

cycle components. Hence, in order to detect robust multi-decadal climatic trends, time-series should span significantly longer than 3 decades. The salinity time series used here, based on the EN3 monthly dataset, span a 60-year period (1950–2010), which is probably sufficient for filtering out intra-decadal and most of multi-decadal natural climate oscillations. An exception may be the AMO, for which many studies show a second variability peak in the 60–75 years range (e.g. Sutton and Hodson 2003; Kavvada et al. 2013), suggesting a potential AMO footprint in the spatial pattern of salinity variability over the EN3 era. Regarding the E–P datasets, only NCEP/NCAR and 20CRv2 reanalyses span the 60-year period and can be compared with the entire salinity time series. An important caveat is that the salinity and E–P data are considerably more uncertain during earlier decades in the record, due to poor spatiotemporal coverage of the data used in the objective analysis for salinity (Ingleby and Huddleston 2007) and in the reanalysis for E–P (mainly through data assimilation of surface products such as SST and Sea Level Pressure). The 1979–2010 time series of salinity and E–P datasets covering the satellite era (along with the other four datasets used here all starting in 1979) are better constrained by in situ observations and satellite-derived data, respectively, and hence they are expected to produce a more spatially coherent global-scale reconstruction of both surface salinity and E–P change patterns, allowing for a more accurate analysis of their co-variability at inter-annual/decadal scales. On the other hand, the 1979–2010 time series are too short in duration for adequately averaging out of multi-decadal fluctuations due to natural variability (e.g. Sohn et al. 2013). Consequently, large-scale natural variability signals should be imprinted in the E–P and surface salinity spatial patterns of multi-decadal change over this period.

Another issue to address when investigating long-term trends in surface salinity is that regional trends are sometimes driven by strong decadal-scale signals which are not always linked to changes in E–P. A typical example of such prominent decadal modes of variability are the Great Salinity Anomalies (GSAs) propagating around the North Atlantic sub-polar gyre over recent decades (i.e. Belkin et al. 1998; Belkin 2004; Wadley and Bigg 2006). In particular, the first and most well-documented of these GSAs is proposed to have been initiated by an anomalously large export of freshwater from the Arctic which advected around the subpolar gyre from 1968 to 1982 (Dickson et al. 1988; Belkin et al. 1998).

Taking these issues into account, we proceed as follows. The first step in our analysis procedure is to construct monthly anomaly time series for all datasets by subtracting the mean seasonal cycle from the monthly data at each grid point. Annual anomalies are then constructed from the

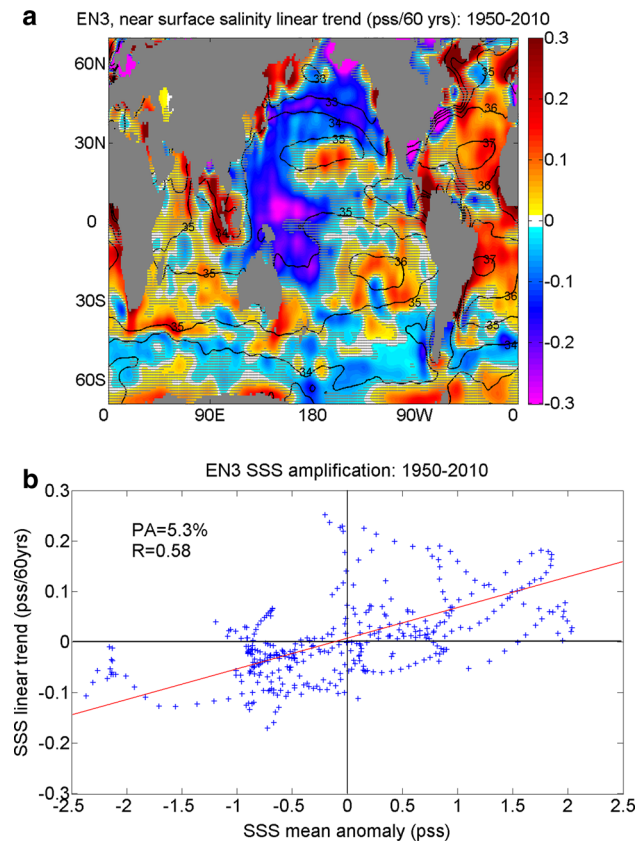


Fig. 2 **a** Linear trend in near surface salinity (pss/60 years) over 1950–2010. Climatological mean salinity contours are plotted every 1.0. Regions where the linear trend is not significant at the 95 % confidence level are stippled in gray. **b** Amplification of the near surface salinity mean field over 1950–2010. The pattern amplification (PA) and correlation coefficient (R) are also depicted

monthly anomalies, allowing us to compute linear trends and S/E–P correlations for both 1950–2010 and 1979–2010 time series. In the following sub-sections, we first consider separately the changes of salinity and freshwater fluxes, then the evidence for any links between these changes, and finally infer changes in freshwater fluxes from the changes in salinity.

3.1 Observed changes in salinity and freshwater fluxes

3.1.1 Near-surface salinity changes

The spatial pattern of near-surface salinity linear trend over 1950–2010 (Fig. 2a) obtained here is quite similar to both the near-surface salinity and E–P climatological mean patterns (not shown), denoting a general broad-scale amplification of the mean salinity field and clearly suggesting a strengthening of the global oceanic water cycle as previously shown by Durack et al. (2012) over the 1950–2000 period. Fresh regions become fresher and salty

regions become saltier. That is consistent with the “wet regions become wetter and dry regions become drier” for the earth’s surface freshwater budget as observed over the last few decades and predicted by coupled climate models in response to global warming (e.g. Chou et al. 2009). Statistically significant and spatially coherent positive salinity trends are found in many evaporation-dominated regions such as the subtropical gyres of all three major oceanic basins whereas decreasing salinity trends are found in precipitation-dominated regions such as the western Pacific Warm Pool and the North Pacific subpolar region. Coherent freshening across large expanses of the mid-latitude Southern Ocean is subject to considerable uncertainty.

There are a few exceptions to this amplified spatial pattern, such as the fresh tropical East Indian Ocean and North Atlantic subpolar regions, where instead multi-decadal increasing salinity trends are observed. Salinity gain is also obtained in most areas around Antarctica ($>60^{\circ}\text{S}$), although confidence in this trend is again severely limited by sparse observations in this region (see Fig. 1). These near-surface salinity changes should naturally be compared with the results of previous studies, taking important caveats into account. Boyer et al. (2005) computed salinity trends over 1955–1998 based on pentadal salinity anomalies derived from the World Ocean Database 2001 (WOD01). Hosoda et al. (2009) estimated the global upper 100 m layer salinity change between WOD05 1960–1989 climatology and ARGO 2003–2007 climatology. Durack and Wijffels (2010) used various observational sources covering the period 1950–2008 to compute 50-year trends over the nominal 1950–2000 period. In the latter study, unlike the other analyses in which trends are linearly fitted to the interpolated data provided by the objectively analysed fields, the salinity trends were fitted concurrently with the mean climatology and the ENSO signal through a multiple linear regression using the available observations in each grid cell ($1^{\circ} \times 2^{\circ}$ grid). Durack and Wijffels (2010) further used a variable search radius, dependent on spatial and temporal sampling, which leads to highly-variable “spatial footprints” of mapped trends in the pre-Argo era (largest in the Southern Ocean, smallest in the North Atlantic), and broad-scale trends are appropriately emphasized.

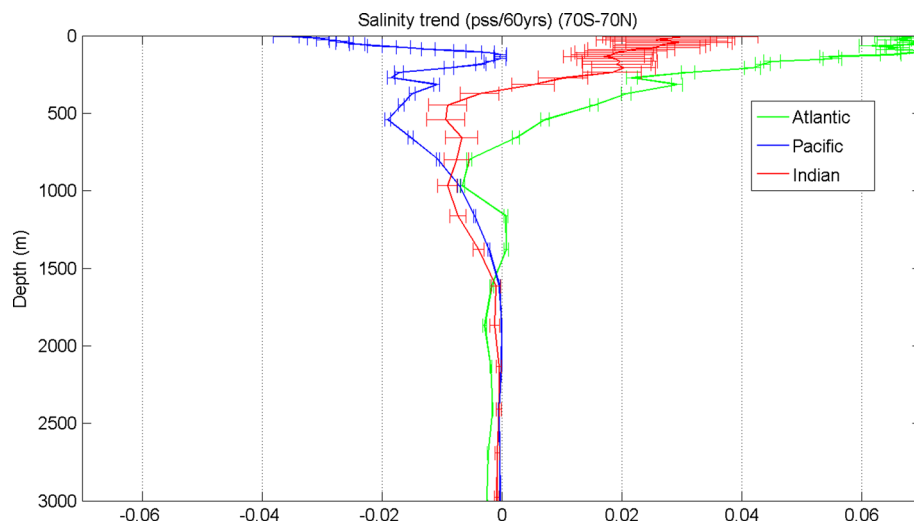
Despite the different methods, assumptions and periods used to compute the salinity change, our results compare favourably with these previous analyses, showing the same general spatial structure of multi-decadal surface salinity change, reflecting the broad-scale amplification of the mean field. In particular large-scale features common to all studies include the general salinity increases in the subtropical gyres, the strong and almost basin-scale surface salinification of the Atlantic Ocean, the large freshening of

the western Pacific Warm Pool and the North Pacific subpolar regions. However there are some noteworthy regional differences between the various analyses. In contrast to long-term freshening of the North Atlantic subpolar region in Boyer et al. (2005), surface salinity gain is observed for this region in the present study, as also in Hosoda et al. (2009) and Durack and Wijffels (2010). This trend is predominantly associated with strong and persistent salinity increase over roughly 1990–2010, following a long period of relatively low salinity (Holliday et al. 2008; Reverdin 2010), that was associated with the Great Salinity Anomaly (e.g. Dickson et al. 1988; Belkin et al. 1998). The freshening trend of Boyer et al. (2005) is therefore a consequence of using a shorter time series (up to 1998). Another notable large-scale difference in the spatial patterns of multi-decadal surface change is encountered in the tropical Indian Ocean (10°S – 10°N , where a clear freshening signal is obtained in Durack and Wijffels (2010) as opposed to an increasing salinity trend in our analysis [as well as in the analysis of Boyer et al. (2005)]. Similarly to the Southern Ocean, the interior Indian Ocean is a region of sparse data coverage, resulting in large uncertainties in long-term trends (Durack and Wijffels 2010).

To quantify amplification of the surface salinity mean field, Durack et al. (2012) introduced the notion of pattern amplification (PA), defined by the slope of the linear regression of basin zonal-mean SSS change against the local SSS anomaly with respect to global-mean SSS, with the correlation coefficient of the linear regression indicating statistical robustness of the PA. Our 60-year PA is about 5.3 % ($r = 0.57$, $p < 0.05$)—see Fig. 2b. In accordance with Durack et al. (2012), marginal seas are excluded from the analysis, as SSS in such regions is strongly influenced by local runoff and variable exchanges with the open ocean.

When we scale the salinity changes to represent 50-year trends, the PA is about 4.5 %, close to the values derived by both Hosoda et al. and Boyer et al. analyses (~ 5 %) as well as to that of the CMIP3 historic simulations ensemble mean (~ 4 %) over 1950–2000 (Durack et al. 2012). However, our 50-year PA value is significantly lower than that obtained by Durack et al. over the nominal period 1950–2000 (~ 8 %), with the corresponding correlation coefficient also weaker (0.58 vs. 0.71), denoting a less spatially coherent amplification pattern. In general then, our multi-decadal salinity anomalies are weaker compared with Durack and Wijffels (2010). This could be a result of the objective analysis used to generate the EN3 dataset (the same applies to the studies of Boyer et al. and Hosoda et al.). The interpolation procedure in the objective analysis, particularly in areas of poor observational spatio-temporal coverage such as the Southern Ocean, may result in the underestimation of salinity anomalies (e.g. Gouretski

Fig. 3 Basin-average profile of salinity trend (pss/60 years) in the three major basins (70S–70 N). Standard error bars are also shown



and Koltermann 2007; Gille 2008). This is probably accentuated further by the monthly grid cell values used in the EN3 dataset, as opposed to the methodology of Durack and Wijffels (2010), which uses decadal bins and focuses on broad-scale footprints.

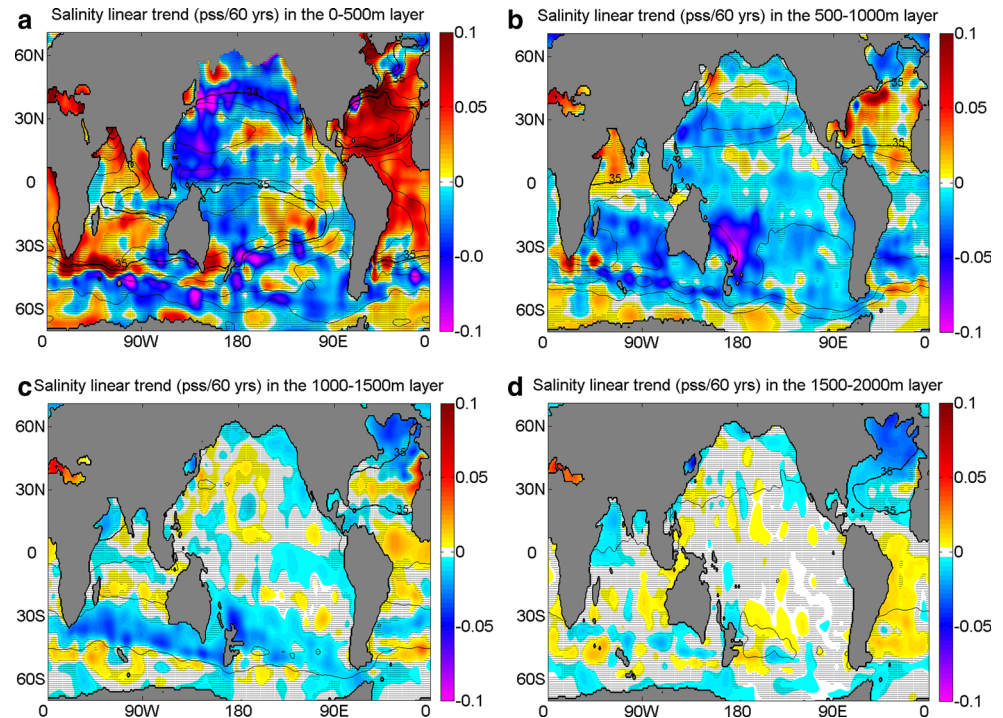
3.1.2 Sub-surface salinity changes

Partitioned by ocean basin, Fig. 3 shows that on average the Atlantic is becoming more saline, while the Pacific is freshening, and the Indian Ocean is gaining and losing salt above and below ~ 400 m, respectively. Average-basin profiles highlight the amplification of the salinity contrast between salty upper thermocline and fresh intermediate waters (~ 500 – $1,000$ m) in all three basins. The 3-D global ocean pattern of salinity change obtained here is qualitatively comparable to that obtained by Boyer et al. (2005) for the period 1955–1998 and by Durack and Wijffels (2010) for the period 1950–2008 although again some regional differences exist that are probably due to the different periods and methods/assumptions considered in the trend analysis. Globally integrated, salinity change is estimated at $\sim 2 \times 10^{-4}$ pss per 60 years, essentially zero within our error margins (a value of zero assumes negligible dilution of the World Ocean over the same period). Long-term trends in some regions of the deep ocean—while hard to distinguish from measurement errors and large changes in full-depth sampling—may be real. For example, a discernible negative “offset” in the 1,500–3,000 m layer of the Atlantic Ocean is largely compensated by the large salinity gain of the upper 500 m.

Salinity changes are evident throughout the upper 2,000 m (Fig. 4). In the upper 500 m (Fig. 4a), encompassing the upper thermocline, trends closely resemble

those at the surface but a stronger amplification of the salinity contrast between the Atlantic and Pacific Oceans is evident. In the Atlantic, salinity gain is found almost everywhere between 30°S and 50°N , whereas the Pacific sees almost basin-wide freshening. The broad-scale freshening featured in the upper 500 m layer of the North Atlantic sub-polar region in Boyer et al. (2005) is not obtained here, in agreement with Durack and Wijffels (2010). Terray et al. (2012) showed that strong amplification of the tropical/subtropical Atlantic–Pacific surface salinity contrast from the early 1970s to late 2000s significantly exceeded internal natural variability in several control CMIP3 simulations, while the pattern bears strong resemblance to anthropogenic responses in transient twenty-first century simulations. An intensifying contrast between Atlantic and Pacific salinity is consistent with enhanced water vapour transport from the tropical Atlantic to the Pacific in response to broad-scale warming (Richter and Xie 2010). Other thermocline changes are noteworthy. Strong salinity gain in the southwest Indian Ocean, coincident with the Agulhas Current system, suggest that strengthening Agulhas leakage (of high-salinity Indian Ocean thermocline waters) may account for some of the salinity gain seen in the South Atlantic. Strong upper ocean salinity gain is also evident in strongly evaporative marginal seas such as the Mediterranean Sea, in agreement with observational studies of long-term salinity changes in this region (e.g. Rixen et al. 2005). In the Southern Ocean, a broad-scale freshening pattern is observed in the Pacific and Indian sectors, in agreement with Durack and Wijffels (2010), but confidence in these trends is severely limited by sparse observations (see Fig. 1). There is a notable difference with the analysis of Boyer et al. (2005), in which a broad-scale salinification is evidenced in the upper 500 m layer of the Indian Sector of the Southern Ocean.

Fig. 4 Salinity linear trend (pss/60 years) over 1950–2010 in four depth layers: **a** 0–500 m; **b** 500–1 000 m; **c** 1 000–1 500 m; **d** 1 500–2 000 m. Climatological mean salinity contours are plotted every 0.2. Regions where the linear trend is not significant at the 95 % confidence level are stippled in gray



In the underlying 500–1,000 m layer (Fig. 4b) the widespread trend is freshening, with notable exceptions of the subtropical North Atlantic and the Mediterranean Sea, where salinity gain persists. The largest freshening trend in this layer, in the southwest subtropical Pacific, exceeds -0.1 pss over 60 years. Patches of weak positive trend are found around Antarctica, but again confidence in these trends is very limited. In the 1,000–1,500 m layer (Fig. 4c), freshening is more clearly associated with Subantarctic and Subpolar mode waters. By 1,500–2,000 m (Fig. 4d), the dominant freshening trend in the global ocean is restricted to subpolar mode water in the North Atlantic while a basin-wide salinity gain appears in the South Atlantic, but limited sampling at these depths again restricts confidence.

The 3-D patterns of salinity change indicate propagation pathways into the ocean interior, and corresponding time-scales, that are broadly consistent with the large-scale circulation. Salinity anomalies in lower thermocline waters at low latitudes can be traced to intermediate water masses ventilating at higher latitudes and propagating equatorward along isopycnal surfaces. Recognising changes in water masses, specifically on isopycnals, Fig. 5 shows salinity changes on local sub-surface maxima and minima in mean salinity, as representative of upper thermocline and intermediate waters respectively. This confirms that upper thermocline (intermediate) waters are gaining (losing) salt content almost everywhere in the global ocean, in accordance with the findings of Helm et al. (2010) over 1970–2005 (see their Fig. 2a, b). The largest

salinity gain in upper thermocline waters occurs within the tropical Atlantic while the largest freshening in intermediate waters occurs in the South Indian and North Pacific subtropical gyres, in agreement with Helm et al. (2010).

Figure 6 shows the 60-year salinity change zonally averaged in latitudinal sections across the three major ocean basins. A repeated pattern in each southern hemisphere subtropical region is the freshening signal coincident with subduction into the Southern Ocean thermocline, following the pathways of SAMW and AAIW along isopycnals at intermediate depths. This broad-scale freshening pattern at intermediate depths of the southern hemisphere is also clearly featured in the trend analyses of Durack and Wijffels (2010) (see their Fig. 7a, d, g) and Helm et al. (2010) (see their Fig. 3c) but it is not evidenced in Boyer et al. (2005), which did not benefit from the enhanced data coverage provided by the ARGO programme. Underlying this freshening pathway in the South Atlantic we find a layer of increasing salinity that extends from the surface Southern Ocean around $50\text{--}60^\circ\text{S}$ to the subtropics and tropics of the South Atlantic at 1,200–2,000 m (see Fig. 6a), in agreement with Durack and Wijffels (2010). Although limited sampling in this region (see Fig. 1) restricts again confidence in the long-term trend, the salinity gain of this layer may be linked to a southward shift of the Antarctic Circumpolar Current (ACC) front (Alory et al. 2007; Gille 2002). The shift of the outcropping isopycnals around the ACC front to either fresher or saltier surface regions within the Southern Ocean may result in

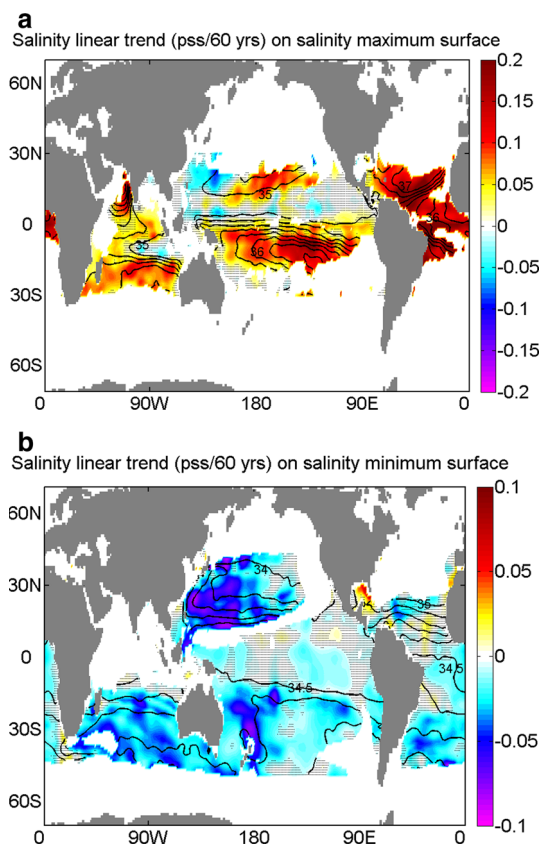


Fig. 5 Salinity linear trend (pss/60 years) on (*vertically*) local sub-surface maxima (**a**) and minima (**b**) in mean salinity. Climatological mean salinity contours are plotted every 0.5. Regions where the linear trend is not significant at the 95 % confidence level are stippled in gray

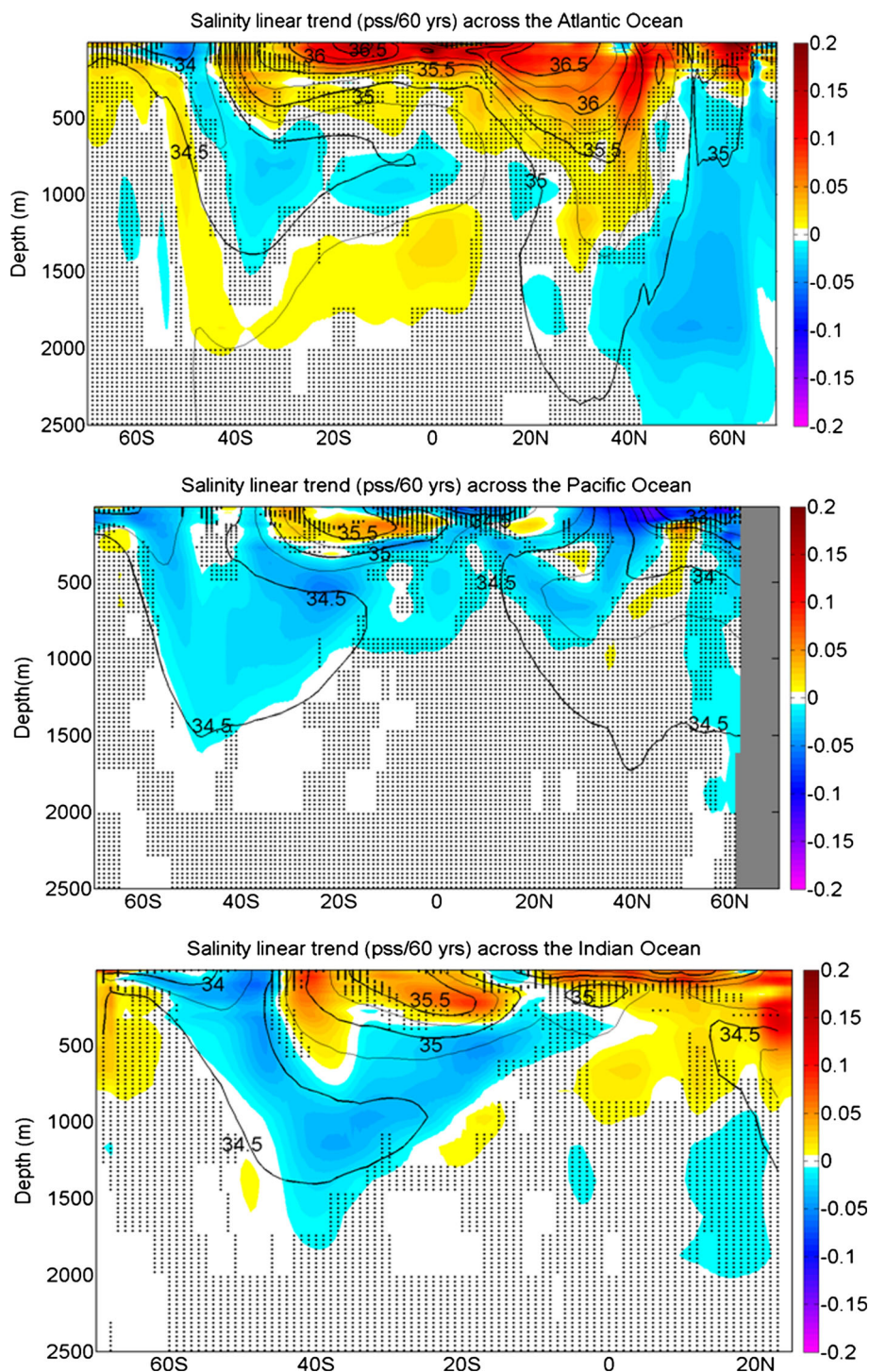
strong salinity anomalies being propagated along isopycnal surfaces to deeper parts of the subtropical/tropical regions.

Below 1,000 m in the North Atlantic, a pronounced dipole of multi-decadal salinity anomalies (magnitude exceeding 0.05 pss) suggests the propagation of distinct water mass signals characterised by strong trends of opposite sign: a salinity gain signal associated with the Mediterranean outflow at 1,000–1,500 m depth propagating both south-westward into the central North Atlantic and northward along the European continental slope, and a freshening signal associated with the Labrador Sea Water (LSW) propagating southward from the northern North Atlantic and through the subpolar gyre to the subtropics (see Fig. 4c). A large dilution of the Northern North Atlantic sub-polar areas and the Nordic Seas down to 2,000 m depth took place between the mid-1960s and the mid-1990s, mainly linked to the GSAs (Curry and Mauritzen 2005; Boyer et al. 2007). Conversely, the Mediterranean Sea underwent a strong salinity gain over the second half of the twentieth century, attributed to large changes in the air-sea freshwater fluxes and a drastic

reduction of river freshwater inputs associated with damming (Rohling and Bryden 1992; Bethoux and Gentili 1999; Skliris et al. 2007). Our results show that below 1,000 m, the Mediterranean basin underwent the strongest salinity gain anywhere in the World Ocean over 1950–2010 (>0.05 pss over 60 years in the 1,000–1,500 m layer, see Fig. 4c). There is a discernible trend of increased salinity in key Mediterranean intermediate and deep water masses and this “Mediterranean signal” of change is also clearly imprinted in the North Atlantic intermediate waters through the propagation of the Mediterranean Overflow Water (MOW) (Curry et al. 2003; Potter and Lozier 2004; Bindoff et al. 2007; Durack and Wijffels 2010). The northward branch of MOW eventually reaches the North Atlantic deep water formation sites, providing high salinity waters that may contribute to the preconditioning of North Atlantic Deep Water, potentially playing a significant role in the global meridional overturning circulation (Reid 1979; McCartney and Mauritzen 2001). However, the salinity gain signal associated with the northward MOW branch obtained here is of limited extent, and does not reach the subpolar gyre (see Fig. 4c). The northward penetration of MOW was recently shown to be an intermittent feature, depending upon the expansion/contraction of the North Atlantic subpolar gyre and the location of the subpolar front, which is in turn shown to vary with the NAO (Lozier and Stewart 2008). During the persistent increasing positive-phase NAO period of the 1960s–early 1990s, the subpolar front moved eastward, essentially blocking the northward-flowing MOW and preventing its entry to the subpolar gyre (Lozier and Stewart 2008).

Figure 7 shows annual layer-averaged salinity anomalies in the subtropical and subpolar gyres of the North Atlantic, in the upper ocean (0–500 m, Fig. 7a) and at the depth of North Atlantic Deep Water (1,500–2,000 m, Fig. 7b). A clear impression from these time series is predominant decadal variation, with opposing changes in upper and deep layers, and significant correlation between changes in the two gyres, consistent with rapid meridional advection of salinity anomalies. Although the North Atlantic sub-polar region underwent salinity gain during the last two decades, the large freshening signal that occurred in the 1970s–1980s during the Great Salinity Minimum period (Dickson 1988; Belkin et al. 1998) seems to be propagating until at least the early 2000s in the subtropical North Atlantic down to 2,000 m depth. Relatively strong positive correlations ($r > 0.65$, $p < 0.01$) were obtained between annual salinity anomalies in the subpolar and subtropical gyre, in both the upper 500 m and the deep 1,500–2,000 m layer, suggesting that salt advection plays a major role in controlling salinity changes in the North Atlantic. The salinity increase in the upper 500 m of the subpolar gyre over recent decades closely follows that

Fig. 6 Averaged salinity linear trend (pss/60 years) over 1950–2010 in latitudinal sections across the three major ocean basins: **a** Atlantic ocean; **b** Pacific ocean; **c** Indian Ocean. Climatological mean salinity contours are plotted every 0.25. Regions where the linear trend is not significant at the 95 % confidence level are stippled in gray



of the subtropical gyre, whereas the subtropical gyre freshening signal at 1,500–2,000 m follows that of the sub-polar gyre, with a maximum correlation lag of 7 years. Unlike the North Atlantic, the poorly-ventilated North Pacific underwent much weaker changes in intermediate/deep layers, with the signal of change concentrated at shallow depths. This is consistent with Ekman suction as a

primary influence on the variability of sub-surface water mass properties.

In summary here, our analysis of sub-surface salinity changes reproduces the main results of Helm et al. (2010) and Durack and Wijffels (2010), including the increased salinity contrast between the upper layer Atlantic and Pacific oceans and between the upper thermocline salinity

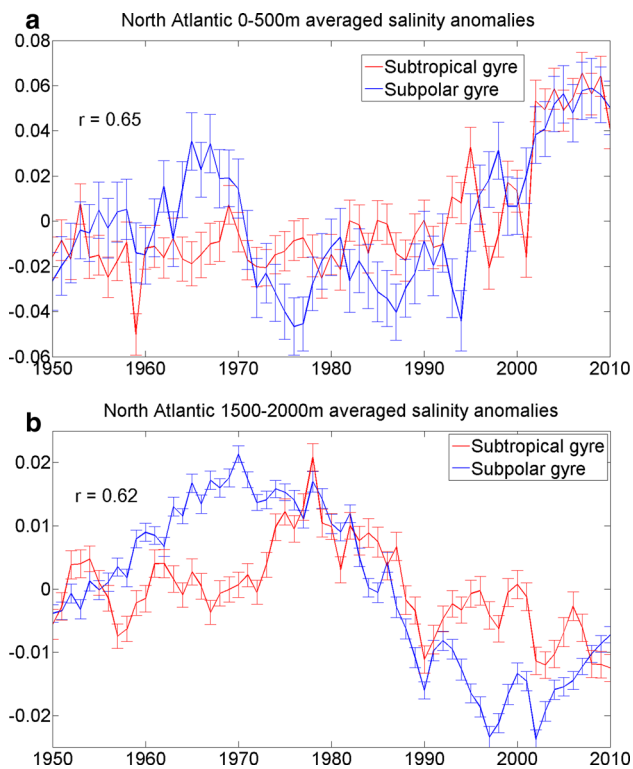


Fig. 7 Annual layer-averaged salinity anomalies in the subtropical and subpolar gyres of the North Atlantic: **a** 0–500 m; **b** 1 500–2 000 m. Correlation coefficients between the time series and standard error bars are also shown

maximum and the salinity minimum of intermediate waters. This further strengthens the case that long-term change of the 3-D salinity field, as assessed from several independent studies that have considered different datasets, time periods and many different analysis assumptions, underscores that oceanic water cycle change is very likely to have occurred over the observational record.

3.1.3 *E–P* changes

A common problem when estimating long-term trends in the *E–P* field using re-analyses or blended re-analysis/satellite-derived products is the inhomogeneities arising in the time series due to the changing observing system and the inclusion of new (mainly satellite) data sources (e.g. Trenberth et al. 2005; Yu et al. 2008; Schanze et al. 2010). Major transition events in data composition include the beginning of the Outgoing Longwave Radiation (OLR) Precipitation Index (OPI) mission (1979), changes attributed to the availability of AVHRR SST data (1982 and 1985), and, in particular, the inclusion of SSM/I data (1987), which greatly increased spatial and temporal resolution in these datasets (Schanze et al. 2010). As a consequence, analysis for both 1950–2010 and 1979–2010

periods considered herein is affected by these discontinuities in data composition, compromising trend estimates. With this caveat in mind, we first consider changes in *E–P* over the 60-year period since 1950. At this timescale there are just two atmospheric reanalyses available, NCEP/NCAR and 20CRv2, and unfortunately these are not independent. The lack of independence arises because the 20CRv2 makes use of an NCEP numerical weather prediction model. The primary difference between the two is that 20CRv2 assimilates a restricted range of data types (just sea level pressure with SST as a boundary condition) whereas input data to NCEP/NCAR covers a wide range of variables (Compo et al. 2011; Kistler et al. 2001). Taking this issue into account, we examine *E–P* trends in the two datasets, expecting a reasonable level of agreement due to the lack of independence.

Figure 8 shows global ocean spatial patterns of 1950–2010 linear trends in *E–P*, *E*, and *P*, for 20CRv2 and NCEP/NCAR. The two products agree in the sign of *E–P* trend (Fig. 8c) at about 65 % of ocean grid points, but agreement at this level or greater is to be expected given that they are not independent, so this should not be interpreted as providing support for the trends shown. Moreover, only about half of these grid points showing sign agreement present statistically significant trends in both products. Large regions characterised by trends that are opposite in sign are found in the tropics with a reasonable level of co-ordination in the location of these regions between the two products but some areas of notable disagreement, in particular the tropical Atlantic. The southern hemisphere subtropics tend to exhibit a positive trend in *E–P* and the Southern Ocean and sub-polar regions a negative trend. Large differences in the *E–P* trend patterns between the two products are evident in a number of regions, particularly the North Atlantic. This is of particular concern given the use of NCEP NWP models for each product and suggests low confidence in the trends at 60-year timescales. Note also that the 60-year changes in *E–P* are much less spatially coherent than those in SSS discussed earlier.

Considering the individual terms, the level of agreement between the two products is comparable for *E* (64 % sign agreement, root mean square difference (rmsd) = 0.18 m/year) and *P* (65 % sign agreement, rmsd = 0.26 m/year) (Fig. 8f, i). For both products, the major contributor to the 60-year change in *E–P* is the precipitation field. The precipitation trend is larger than the evaporation trend at 62 and 61 % of ocean grid points for 20CRv2 and NCEP/NCAR reanalyses, respectively. Especially in the tropical region, where the largest variability signals occur, precipitation clearly drives *E–P* changes, whereas the contribution of the evaporation field to *E–P* change is mainly concentrated in the subtropical regions.

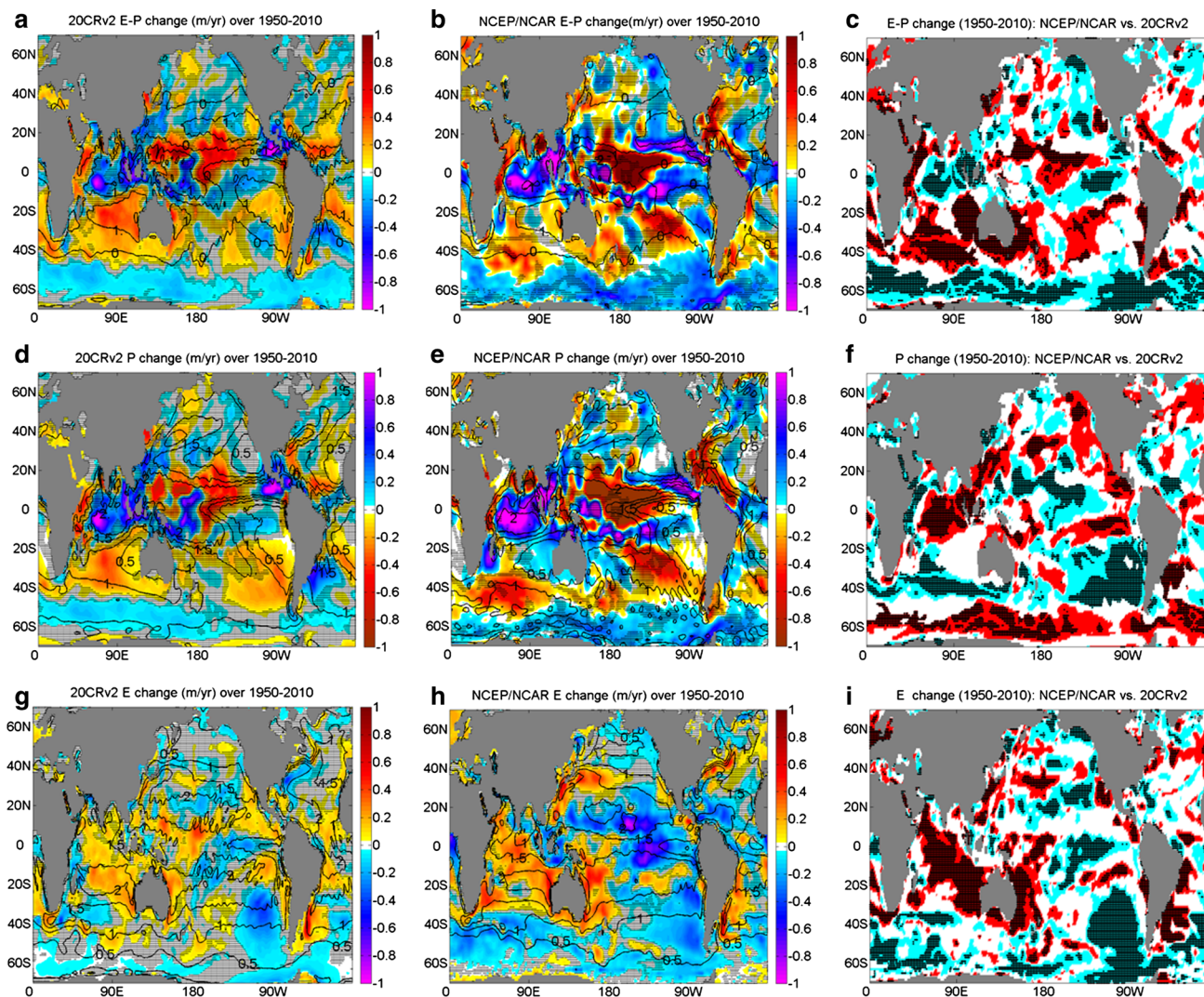


Fig. 8 E–P, E and P linear trend (m/year/60 years) spatial pattern over 1950–2010, in 20CRv2 (**a**, **d**, **g**) and NCEP/NCAR (**b**, **e**, **h**). Regions where the linear trend is not significant at the 95 % confidence level are stippled in gray. Climatological mean E–P contours are plotted every 0.5. The level of trend sign agreement

among the two re-analysis products (**c**, **f**, **i**). *Red colour* indicates common positive trend among the two products, *blue colour* indicates common negative trend and *white colour* indicates no agreement in the trend. Regions where trends from both products are significant at the 95 % confidence level are stippled in *black*

As for near-surface salinity, we have investigated possible amplification of the E–P mean field by computing its PA, i.e. defined by the slope of basin zonal-mean E–P change versus E–P climatological mean (of long-term averages), and the corresponding correlation coefficient of the linear regression for both products (Fig. 9). Both products indicate an amplification of the E–P mean field with the obtained PA for 20CRv2 ($\sim 7\%$, $p < 0.05$) being slightly higher than for NCEP/NCAR ($\sim 6.5\%$). On the other hand, the PA from both re-analysis products is much higher than that for the CMIP3 ensemble mean over 1950–2000 ($\sim 2\%$) (Durack et al. 2012). However, both reanalysis E–P projections show a relatively large spread of the points around the regression line, with the correlation

coefficients being quite small ($R = 0.39$ for 20CRv2, and $R = 0.20$ for NCEP/NCAR) as compared with SSS PA ($R = 0.58$). Hence we have limited confidence in the re-analysis E–P estimates of water cycle intensification.

Some improvement in the reliability of the reanalysis products might be expected from 1979, with the advent of operational satellite observation and the assimilation of satellite data into the models used for the reanalyses. Figure 10 shows the spatial patterns of E–P trend for four reanalysis and two hybrid reanalysis/observations products after 1979. The four reanalyses are NCEP/NCAR (also commonly termed NCEP1), NCEP/DOE (termed NCEP2), 20CRv2 and ERA-Interim. The first three of these all make use of NCEP NWP models and are thus not independent.

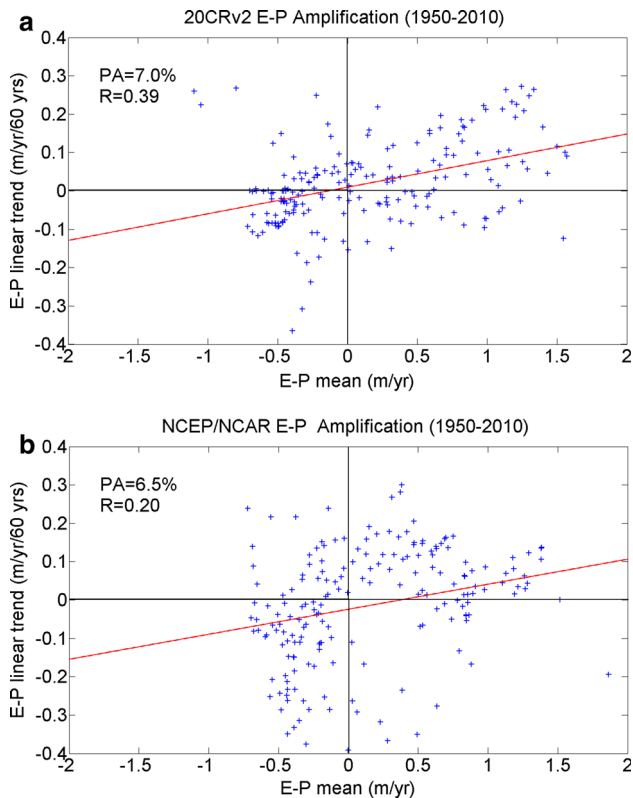


Fig. 9 Amplification of the E–P mean field over 1950–2010 for **a** 20CRv2; **b** NCEP/NCAR. The pattern amplification (PA) and correlation coefficient (R) are also depicted

The two hybrid reanalysis/observations products are COREv2 and OAFlux; unfortunately, in addition to satellite observations, these make use of NCEP/NCAR and ERA40 reanalysis output for the meteorological variables (wind speed, air temperature and humidity, SST) required to determine evaporation. Thus, there is again a lack of independence between the available datasets and this needs to be kept in mind when considering the results presented below.

The results shown in Fig. 10 indicate some coherency in the spatial patterns of change over 1979–2010 across the six products, but also large differences. There is an increase in net precipitation within the tropical convergence zones in the two hybrid observational/reanalysis products (COREv2 and OAFlux/GPCP) and the NCEP-based products, but ERA-Interim shows a largely opposite trend towards increased net evaporation in the tropical Pacific and Indian Oceans. Strong positive E–P trends are evident in the southern hemisphere subtropical regions in all of the products considered. However, elsewhere there are still notable regional differences in both the location and magnitude of E–P changes between the various products. For example, the mid-high latitude North Atlantic shows changes ranging from a strong increase in net evaporation (OAFlux/GPCP) to a strong reduction (NCEP/NCAR).

The level of sign agreement in the E–P trend, when comparing all possible pairs among the six available

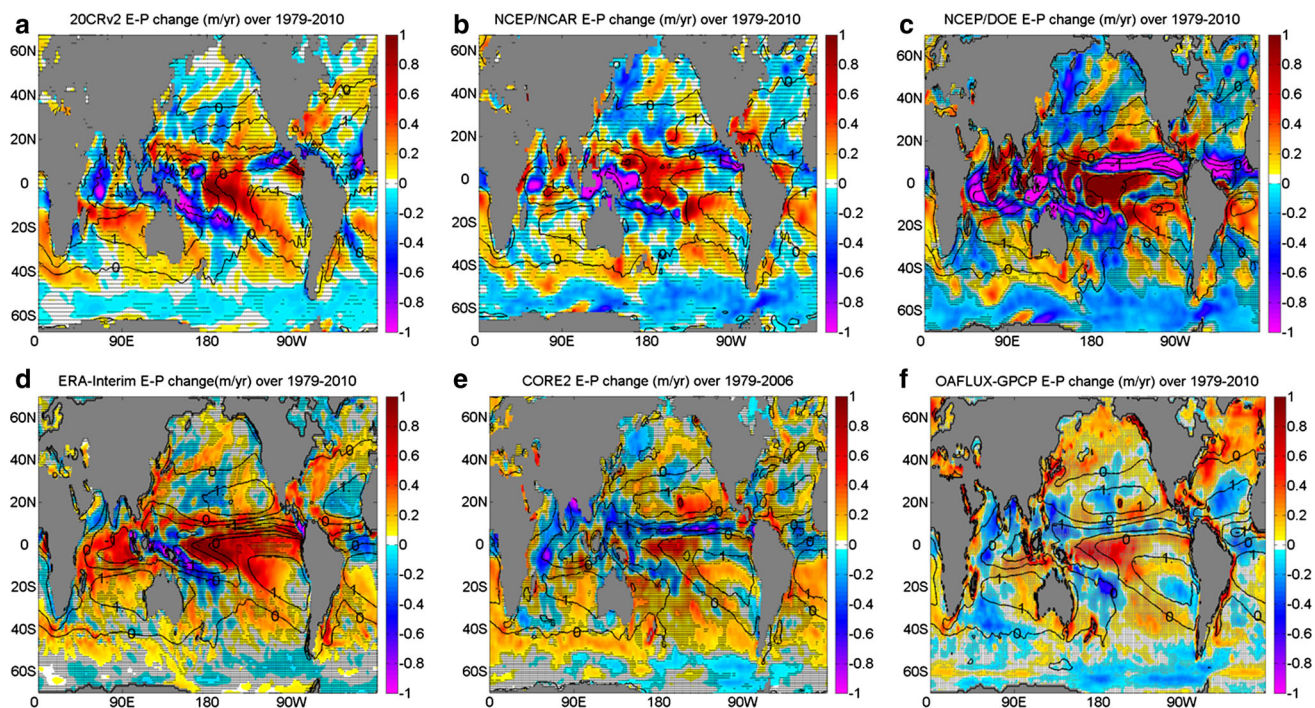


Fig. 10 E–P changes after 1979, in: **a** 20CRv2; **b** NCEP/NCAR; **c** NCEP/DOE; **d** ERA-Interim; **e** COREv2; **f** OAFlux (E)–GPCP (P). Regions where the linear trend is not significant at the 95 %

confidence level are stippled in gray. Climatological mean salinity contours are plotted every 1.0

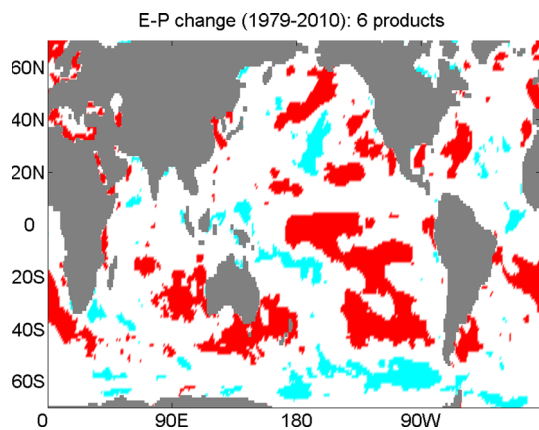


Fig. 11 Level of sign agreement in the E–P trend over 1979–2010 in all six products presented in Fig. 10. *Red colour* indicates common positive trend among products, *blue colour* indicates common negative trend among products and *white colour* indicates no agreement in the trend among products

products, ranges from 55 % (NCEP/NCAR vs. ERA-Interim) to 82 % (NCEP/NCAR vs. NCEP/DOE) and, as expected, it is closely related to the degree of dependency between products. We have attempted to determine regions of consistent E–P trends by investigating the level of sign agreement in the E–P trend in two different combinations of reanalysis/observational products. For this, we have chosen a subset of four products (NCEP/NCAR, OAFflux/GPCP, COREv2 and ERA-Interim), including only one NCEP-based re-analysis and the full set of six products. The level of agreement drops from 33 % when comparing the four-product subset to 25 % when comparing all six products (Fig. 11). The main feature to emerge from the figure is the pattern of increased E–P in all three southern hemisphere subtropical gyres (with the largest signal being evident in the South Pacific), seen in all of the products considered.

The large differences in the spatial patterns of E–P trend among the products are mainly driven by differences in the precipitation field (not shown). In this context, we note again that the change in satellite data sources used in the various reanalysis/observational products within this period seems to be problematic in defining realistic trends (e.g. Schanze et al. 2010; Trenberth et al. 2011). A tendency for more positive trends in ERA-Interim E–P (see Fig. 10d) as compared with the other products may reflect spurious decreases in P over the period, related to the assimilation of satellite observations (John et al. 2009; Dee et al. 2011).

In general, regional precipitation trends are much stronger in reanalysis datasets as compared to GPCP, which is probably associated with too-intense water cycling in most reanalysis models (e.g. Trenberth et al. 2011). There is more consistency between the various

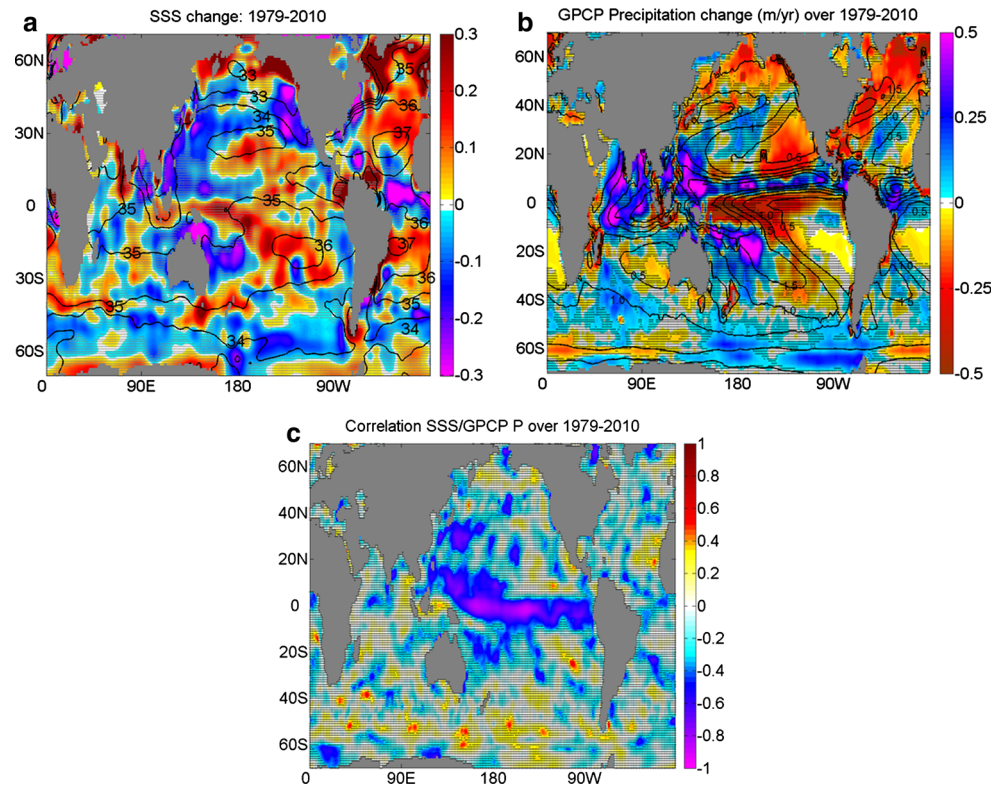
reanalysis products in the spatial patterns of evaporation change (not shown), which are in general strongly constrained by the assimilated satellite-derived SST data. For all products, precipitation change is again larger than evaporation change at the majority of ocean grid points (ranging between 60 and 65 % of ocean grid points for the six E–P products). In summary, the results presented here for E, P and E–P spatiotemporal patterns, derived from global re-analysis/observational datasets, highlight the strong limitations and large discrepancies among these products in representing long-term variability and trends over the ocean, in agreement with previous studies (e.g. Yin et al. 2004; Trenberth et al. 2005; Schanze et al. 2010; Trenberth et al. 2011).

3.2 Linking SSS changes to E–P changes

The spatial distribution of the mean SSS field strongly resembles that of the mean E–P field since the latter is the main driver of its variability. However, the SSS mean presents a much smoother pattern, reflecting the role of ocean advection and mixing in homogenizing air–sea freshwater flux anomalies to restore global freshwater and salt balances (Wijffels 2001). A few recent studies have investigated the relationship between surface salinity and E–P at monthly to inter-annual time scales.

Yu (2011) found major E–P controls on seasonal mixed-layer salinity variability in the tropical convergence zones featuring heavy rainfall, whilst outside the tropics Ekman advection and then vertical entrainment were the dominant processes controlling salinity variability. Vinogradova and Ponte (2013) investigated the link between surface salinity and freshwater fluxes in the global ocean, based on a model/data synthesis of 13 years. They showed that there are only a few regions where salinity can be used as a proxy for freshwater flux, demonstrating the importance of ocean advection and mixing processes in shaping the local and global mean salinity fields. Hasson et al. (2013) investigated mechanisms controlling the mixed-layer salinity in the tropical Pacific during 1990–2009. They demonstrated that all terms of the mixed-layer salinity equation, including high-frequency salinity advection, have to be considered to close the salinity budget, ruling out the use of sea surface salinity to directly infer the mean and seasonal/inter-annual variability of freshwater fluxes. Tzortzi et al. (2013) used one year of spatially dense observations from the SMOS satellite to reveal dominant mechanisms of tropical Atlantic sea surface salinity variability and to investigate links with freshwater flux variability at monthly timescales. The authors found a clear in-phase relationship between SSS and P only in a western pole of strong variability near the Amazon/Orinoco outflow system, emphasizing the importance of ocean advection

Fig. 12 Linear trend (1979–2010) in **a** SSS (Climatological mean salinity contours are plotted every 0.5) and **b** GPCP P (climatological mean E–P contours are plotted every 0.5). **c** Correlations between detrended time series of SSS and GPCP P over 1979–2010. Regions where the linear trend/correlation is not significant at the 95 % confidence level are stippled in *gray*



and mixing elsewhere. At global scale, however, Durack et al. (2012) found a strong relationship between 50-year salinity and E–P changes in an idealized ocean-only model forced by a 5 % linear increase in E–P. These idealised simulations appeared to qualitatively capture the surface and sub-surface broad-scale patterns of salinity change for each basin. The authors also found a similar spatial response to the observed changes in those historical CMIP3 simulations which present strong warming over 1950–2000 (>0.5 °C).

In the present study, we investigate the link between near-surface salinity and E–P at inter-decadal and inter-annual scales. We use both the 1950–2010 time series, which may reveal any link between the spatial patterns of long-term change in the two variables, and the 1979–2010 time series, which is better constrained by the observational coverage and hence it is expected to better represent the co-variability of the two variables at inter-annual/decadal timescales.

The comparison between the spatial patterns of change of SSS (see Fig. 2a) and the two re-analysis E–P products (see Fig. 8a, b) over 1950–2010 shows very limited consistency. There is some consistency in the southern hemisphere subtropical regions, showing a salinity/net evaporation increase, as well as in the high latitude Pacific, showing a freshening trend, but in both cases broad-scale patterns in E–P are much less spatially coherent than those

in SSS. There is also a consistent freshening trend in the Southern Ocean, which is, however, characterised by large uncertainty due to poor spatiotemporal sampling for both parameters. Large discrepancies are found in the North Atlantic, where the strong basin-scale salinity gain is not supported by the E–P change pattern in both reanalyses. Moreover, the well-coordinated widespread freshening in the west part of the tropical Pacific obtained in the SSS change pattern is not produced in that of E–P, the latter showing very strong spatial variability with patches of increasing and decreasing water flux in both reanalyses.

For 1979–2010, greater consistency in the spatial patterns of change between SSS (Fig. 12a) and the various E–P products (see Fig. 10) is obtained. More coordinated broad-scale patterns of increased salinity/net evaporation are found in the southern hemisphere tropical/subtropical evaporative regions. A pronounced dipole of increased salinity/drying and decreased salinity/freshening emerges between the westernmost and central parts of the tropical Pacific, which is a common pattern in all E–P products. However, major discrepancies persist, such as the mid- and high-latitude North Atlantic, where the strong salinity gain is not consistent with the E–P change pattern for all products except for OAFLUX–GPCP.

A way to investigate the local spatial consistency between surface salinity and freshwater flux is to project the spatial pattern of basin zonal-mean near-surface salinity

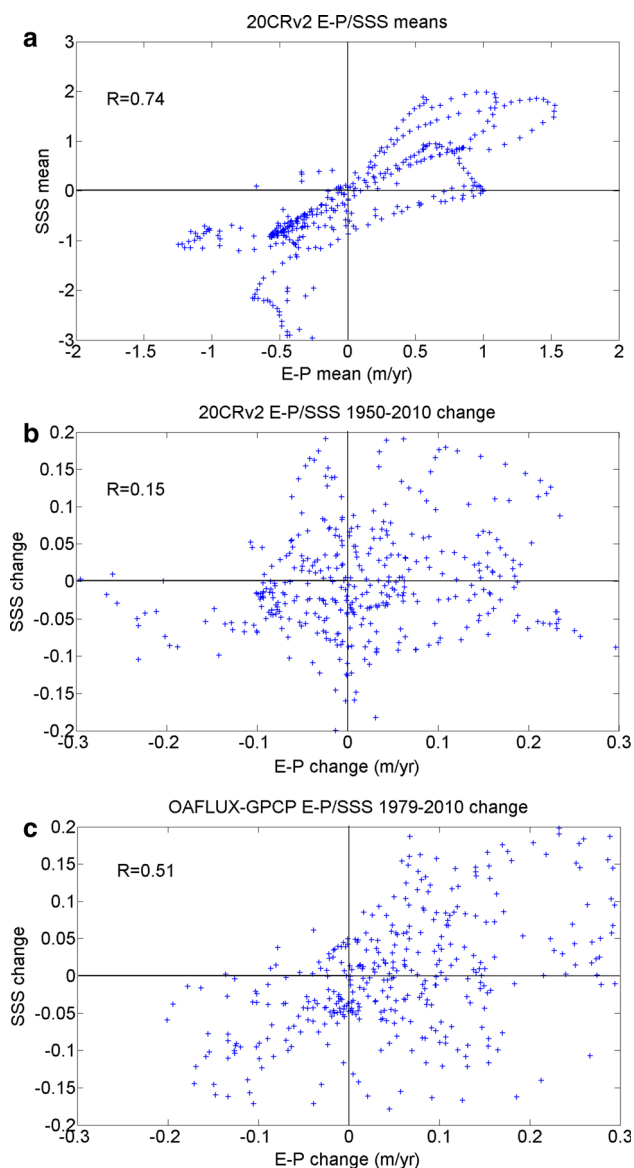


Fig. 13 Projection of the SSS climatological mean and multi-decadal change pattern on the 20CRv2 E-P climatological mean (a) and multi-decadal change pattern (b), respectively, over 1950–2010. c Projection of the SSS multi-decadal change pattern on the OAFLUX-GPCP E-P multi-decadal change pattern over 1979–2010. The correlation coefficient (R) of the linear regression is also depicted

on the pattern of basin zonal-mean E-P for the climatological mean and multi-decadal change (Fig. 13). We have examined this relationship for the two long-term re-analysis products (NCEP/NCAR and 20CRv2). In each case, an overall pattern of increasing salinity with increasing E-P emerges ($r = 0.72$ for NCEP/NCAR and $r = 0.74$ for 20CRv2 (Fig. 13a), both significant at the 95 % level; the similarity of these correlations is to be expected given the lack of independence between 20CRv2 and NCEP/NCAR discussed earlier). This demonstrates the expected

relationship between the spatial patterns of the two water cycle variables.

One may also expect some consistency between the E-P/SSS spatial patterns of multi-decadal change, although ocean circulation and mixing may efficiently propagate salinity anomalies induced by local surface freshwater budget anomalies away from their formation sites, strongly shaping the spatial pattern of salinity change. In addition, uncertainty in the temporal variability of E-P is also likely to make identification of a relationship between SSS and E-P difficult. The correlation coefficients between the SSS and E-P 60-year change (1950–2010) spatial patterns are very low for both NCEP/NCAR ($r = 0.10$) and 20CRv2 ($r = 0.15$) (Fig. 13b), indicating no significant long-term local link between the two variables. If the period is restricted to the more recent interval 1979–2010, similarly low r -values are obtained for all four re-analysis datasets (NCEP/NCAR: $r = 0.11$, 20CRv2: $r = 0.16$, ERA-Interim: $r = 0.07$, NCEP/DOE: $r = 0.15$).

Higher, statistically significant correlations are obtained for the combined re-analysis/observational 1979–2010 datasets i.e. COREv2 ($r = 0.33$, $p < 0.05$) and OAFLUX-GPCP ($r = 0.51$, $p < 0.05$; Fig. 13c). The latter dataset shows the strongest link between SSS and E-P change patterns over 1979–2010, with the correlation coefficient being closer to that of projected E-P/SSS climatological mean patterns ($r = 0.70$). The GPCP dataset is considered by Schanze et al. (2010) to be the state-of-the-art product to study long-term changes in the precipitation field over the global ocean. The OAFlux E dataset has also been shown to be in closer agreement with the limited number of available surface flux buoy estimates (Yu et al. 2008) than various re-analysis products (NCEP/NCAR, NCEP/DOE, ERA-40).

In summary, except for the OAFLUX-GPCP and to a lesser extent for the COREv2 1979–2010 datasets, there is no immediately evident relationship between SSS and E-P change in any of the re-analysis datasets investigated for the two periods considered. This result may point to importance of other physical mechanisms (advection and mixing), inadequacies in the global E-P re-analysis and salinity datasets, different signal to noise ratio in the two variables, or the need for a more sophisticated analysis method to reveal the relationship.

We have also considered potential relationships between SSS and E-P variability at inter-annual timescales, likely to reflect different processes to those associated with any multi-decadal change in the hydrological cycle. In general, higher local inter-annual correlations between SSS and E-P are expected in the tropical convergence zones featuring strong precipitation, whereas low correlations are expected outside the tropics where salt advection and vertical entrainment seem to play a predominant role in locally

shaping the spatial pattern of salinity change (e.g. Yu 2011). Examining local correlations between SSS and E–P annual time series over 1950–2010 and 1979–2010, from both the 20CRv2 and the NCEP/NCAR datasets, we find little evidence for a direct local link between surface salinity and the two reanalysis-derived surface freshwater flux patterns at inter-annual timescales, except for limited areas of significant positive correlation in the tropical Pacific. Stronger correlations and relatively more coordinated spatial patterns are obtained between SSS and 20CRv2 E–P (i.e. as compared with NCEP/NCAR). Some of the poor agreement between E–P and SSS change may be related to limitations in derived fields of both salinity and freshwater fluxes, the products of objective analysis and reanalysis respectively, both strongly dependent on the quality and quantity of the available observations. Until roughly the late 1960s, inter-annual correlations are quite low even in regions where typically the two variables are closely linked such as the West Pacific Warm Pool (i.e. $r < 0.2$ over 1950–1970, $r > 0.5$ over 1970–2010).

A greater level of consistency emerges between the patterns of SSS and both NCEP/NCAR and 20CRv2 E–P change after 1979, evident in the 1979–2010 spatial correlation patterns of the two annual time series (not shown). The stronger correlations between E–P and SSS after 1979 are largely driven by SSS/P co-variability. The most enhanced and spatially coherent correlation patterns over 1979–2010 among all products are obtained between GPCP precipitation and SSS (see Fig. 12). This is particularly evidenced in the tropics, where precipitation clearly dominates the strong E–P trend that is driving the salinity change. We also confirmed this region of robust correlations for the period 1998–2010 using Tropical Rainfall Measurement Mission (TRMM) high-resolution data (not shown). In contrast with P, correlations between E and SSS are generally poor among all reanalysis products, with poorly coordinated patterns of co-variability (not shown).

Figure 14 shows the normalised area-averaged annual anomaly time series of SST, SSS and respectively NCEP/NCAR precipitation and evaporation, in the Western Pacific Warm Pool and the subtropical gyre of the North Atlantic, two regions with a very strong signal of salinity change which is suggested to be an early fingerprint of anthropogenic forcing (e.g. Stott et al. 2008; Terray et al. 2012; Pierce et al. 2012). Results highlight the large evaporation increase/salinity gain in the North Atlantic subtropical gyre and precipitation increase/freshening in the Western Pacific Warm Pool, both highly correlated with the SST increase after the early 1970s and consistent with amplification of the water cycle under global warming. However, it is still difficult to determine if this is a long-term trend in the water cycle components driven by warming or a natural multi-decadal variability signal

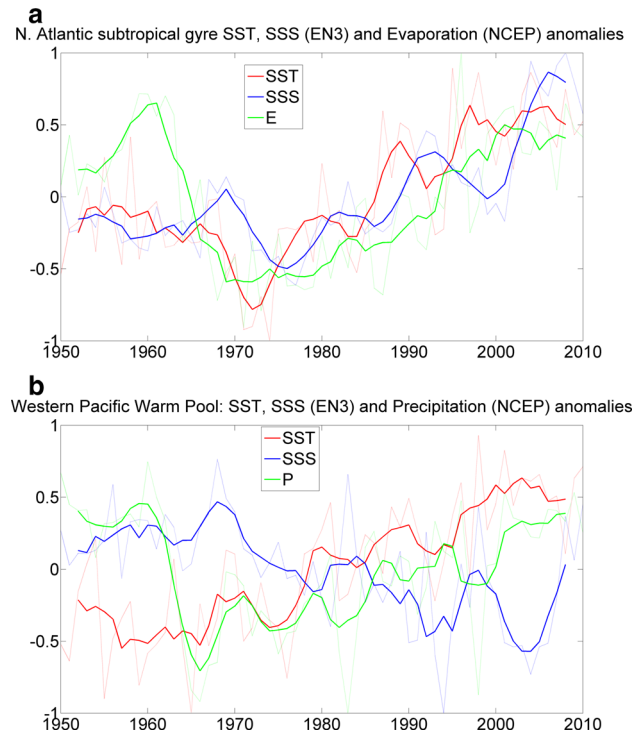


Fig. 14 Normalised (by maximum absolute value) yearly anomalies (*dashed lines*) of near surface temperature (EN3), salinity (EN3) and respectively precipitation and evaporation (NCEP/NCAR), in **a** the Western Pacific Warm Pool and **b** the subtropical gyre of the North Atlantic. 5-year running means (*solid lines*) are also depicted

related to variations in ENSO and/or the atmospheric tropical circulation (e.g. Sohn et al. 2013).

Results show a link in the tropical Pacific over the 1979–2010 period between the spatial change patterns of SSS and E–P that is consistent with enhanced La-Niña conditions, typically evidenced by large freshening of the West Pacific Warm Pool and the Indonesian Throughflow and large drying of the central Pacific. Figure 15a, b shows the correlation spatial patterns between the 1979–2010 time series of Southern Oscillation Index (SOI) and, SSS and P, respectively. There is a clear ENSO imprint on the variability of both parameters involving an out-of-phase oscillation with coherent opposite variation patterns between the central and westernmost parts of the Tropical Pacific. Correlation patterns indicate that SOI variations explain around 30–50 % of SSS and P variability in the central/west tropical Pacific. The SOI annual variations over 1979–2010 (Fig. 15c) shows a period of high negative values indicating prevalent El-Niño conditions with strong El-Niño episodes over roughly the first two decades (peaking at the exceptionally strong El-Niño of 1997/1998) followed by a period of increasing La-Niña (positive values) and less strong El-Niño (low negative values) episodes over the rest of the record. Hence ENSO multi-decadal variability exerts a significant control on the spatial

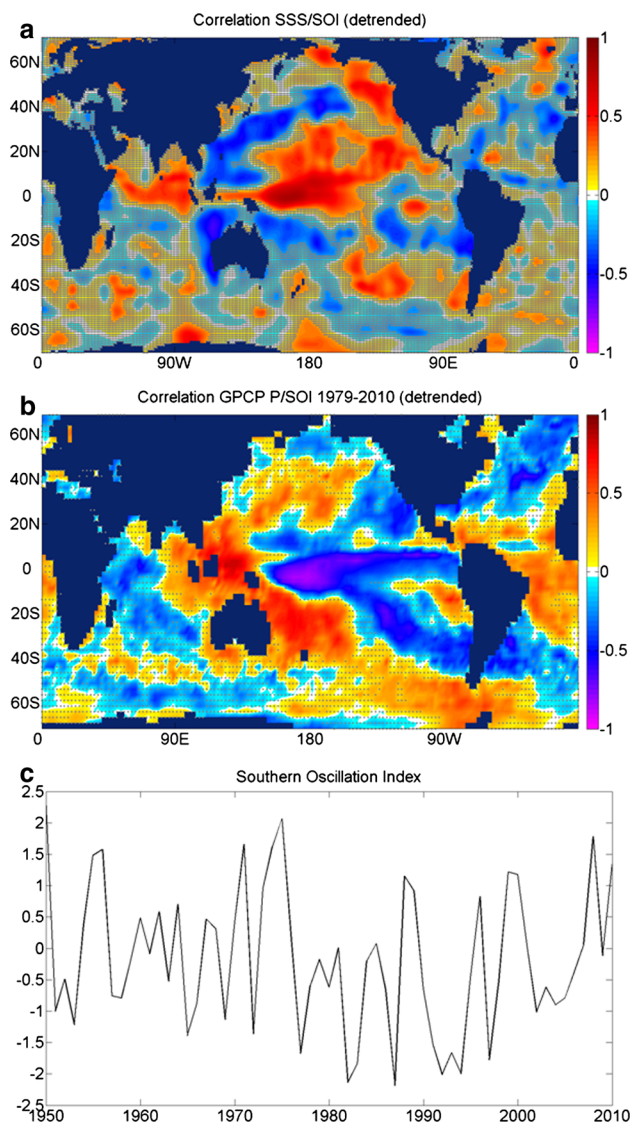


Fig. 15 Spatial patterns of correlation between detrended annual time series of Southern Oscillation Index (SOI) and, **a** SSS (EN3) and **b** precipitation (GPCP). **c** Yearly averaged SOI over 1950–2010

patterns of E–P/SSS linear trends in the tropical Pacific Ocean over 1979–2010. The common SSS/E–P pattern of spatial change obtained here is also quite similar to the spatial pattern of the 3rd leading Empirical Orthogonal Function (EOF) mode of E–P variability obtained by Schanze et al. (2010), who showed that this is the major non-seasonal variability mode of E–P that is highly linked to ENSO. Moreover, there is some observational evidence of a strengthening of the Walker circulation over this period, associated with an increase in the east–west SST gradient in the Tropical Pacific (e.g. Merrifield 2011; Sohn et al. 2013; L’Hereux et al. 2013), which may also partly explain E–P spatial variability in this region.

3.3 Inferring freshwater flux changes from salinity changes

Our study and others in the literature that employ different assumptions (Boyer et al. 2005; Hosoda et al. 2009; Durack and Wijffels 2010; Helm et al. 2010) show similar coherent, broad-scale patterns of salinity change. As shown above, E–P data derived by reanalysis/observational products have much less consistent and less spatially coherent change patterns. Hence, we have more confidence in the observed global pattern of multi-decadal change for salinity than for E–P. Consequently, salinity may provide a more reliable measure than E–P in order to diagnose and quantify the strengthening of the water cycle over the ocean. A few recent studies have inferred long-term surface freshwater flux changes from the observed salinity changes. Hosoda et al. (2009) estimated a global E–P amplification of about 3.7 % from the mid-1970s to mid-2000s using the observed salinity change in the upper 100 m between the WOD05 climatology (spanning 1960–1989) and the ARGO climatology (2003–2007). The authors made the assumptions that the horizontal advection/mixing field is constant and that there is no freshwater/salt exchange below 100 m. The latter is a rather strong assumption taking into account the observed large sub-surface salinity changes at depths exceeding 2,000 m in some regions. Moreover, it is difficult to distinguish the sources of sub-surface salinity changes on pressure surfaces as they are attributable to both isopycnal heave which is mainly driven by wind stress changes, and water-mass modification which is largely driven by changes in the air–sea heat/freshwater fluxes (Bindoff and McDougall 1994).

In contrast, isopycnal surfaces appear to be more natural advective pathways of salinity anomalies as compared with pressure surfaces. Under the assumption that diapycnal mixing in the ocean interior is very weak, sub-surface salinity changes on a particular isopycnal surface may be directly linked to surface salinity anomalies and hence to freshwater flux anomalies at the outcropping region of this isopycnal surface (Bindoff and McDougall 1994). Based on that principle, Helm et al. (2010) inferred the surface freshwater flux change over 1970–2005 by integrating the salinity change and volume along density surfaces from the outcrop region to the equator in each hemisphere. All first-order freshwater changes were assumed to be due to local E–P changes in the extratropics (near-equatorial E–P changes cannot be determined by this method). The authors estimated a 3 ± 2 % increase in net evaporation over the mid and low latitude oceans in both hemispheres, a 7 ± 4 % increase in net precipitation in the Northern Hemisphere high latitudes, and a 16 ± 6 % increase in the Southern Ocean.

However, such analysis may significantly underestimate/overestimate E–P changes, since sub-surface salinity changes on isopycnal surfaces are not only attributed to local surface freshwater budget changes but may be also induced by the horizontal shift in isopycnal outcrops. Over recent decades, there has been a predominantly poleward shift in isopycnal outcrops driven by broad-scale warming (Durack and Wijffels 2010). Poleward migration of an outcropping isopycnal surface towards a fresher region may induce lower salinity being subducted along this particular isopycnal in the sub-surface ocean interior in the absence of local E–P change. Durack and Wijffels (2010) showed that a large fraction of sub-surface salinity changes over 1950–2000 was induced by this warming-driven migration of isopycnal surface outcrops. Moreover, salinity changes in deeper layers of the major ocean basins may also be driven by the T–S modification of inflowing water masses, e.g. Mediterranean outflow and dense overflows at higher latitudes in the North Atlantic, and Red Sea/Persian Gulf overflows in the Indian Ocean.

Another drawback of both the aforementioned studies is that they used a relatively short period to infer freshwater flux changes (~ 30 – 35 years), with natural decadal modes of variability probably dominating a significant part of the observed salinity change. In a recent study, Durack et al. (2012) used an indirect method to infer the rate of global water cycle intensification over 1950–2000 from the PA of the observed SSS, and PAs for SSS and E–P in the ensemble of CMIP3 simulations. Using the CMIP3 model relationships between PAs for SSS and E–P, Durack et al. (2012) established that the PA for SSS increases at twice the rate of the PA for E–P. Applying this relationship to their observed SSS PA estimate of $\sim 8\%$, they inferred that the global water cycle has amplified by $\sim 4\%$ over 1950–2000. However, apart from the observed salinity change, the accuracy of this method depends on the ability of CMIP3 models to properly simulate the response of both E–P and SSS to warming. CMIP3 historic simulations present much less consistent and robust results regarding the relationship between E–P/SSS PA and SST change, with a large spread between models especially at low warming rates. Importantly, the CMIP3 ensemble mean shows a 50% weaker surface salinity PA over the second half of the twentieth century/early twenty-first century as compared to that observed by Durack et al. (2012).

In the present study we use an alternative method to infer the yearly E–P change from the yearly volume-averaged salinity change in a volume bounded by the sea surface and specific neutral density surfaces, using an approximate salt conservation equation:

$$\rho_t S_t V_t = \rho_{t+\Delta t} S_{t+\Delta t} (V_t + hA_t) \quad (1)$$

where ρ is in situ volume and annually-averaged density (kg m^{-3}), S is the volume and annually-averaged salinity,

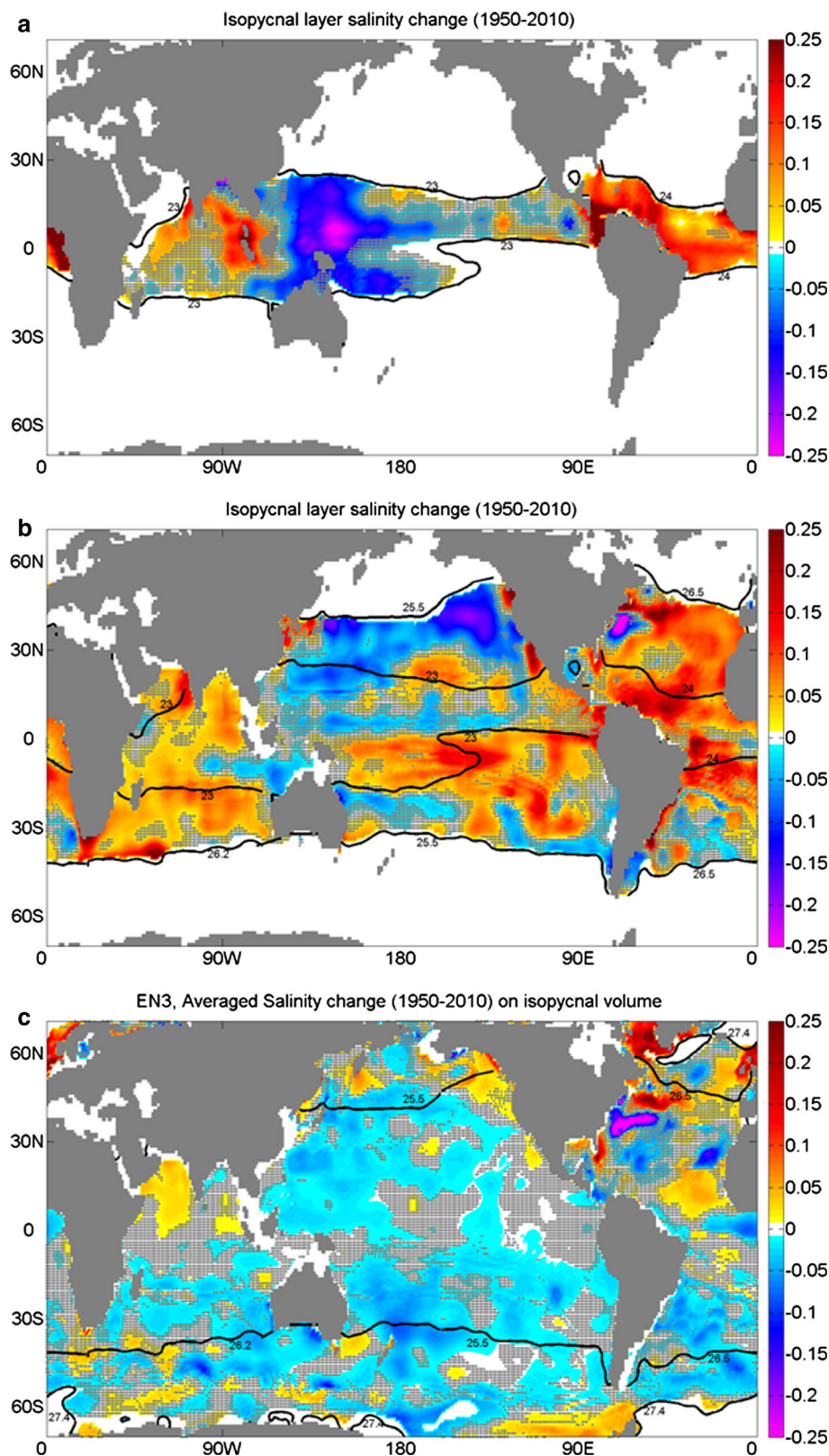
V is the annually-averaged volume of integration bounded by the sea surface and chosen neutral density surfaces, t is time (year), Δt is an integration time step ($=1$ year), A is the sea surface area of integration bounded by the neutral density surface outcrops, and h is the annually-averaged height (m) per unit area of freshwater accumulated or lost at the surface due to change in the surface freshwater flux. Hence the inferred E–P change (m/year) over time Δt is given by $h/\Delta t$.

The advantage of this method is that yearly horizontal/vertical shifts of isopycnal surfaces are explicitly taken into account in the salt content computations. The outcropping locations of a neutral density surface and hence the horizontal sea surface extent of the area of integration are allowed to vary from one year to another. It is important to thus account for the horizontal migration of isopycnal surface outcrops, which is shown to induce large sub-surface salinity changes (Durack and Wijffels 2010). However, E–P changes cannot be resolved as zonal averages or for specific regions separately for each hemisphere using this method.

By knowing the approximate locations of isopycnal outcrops in each oceanic basin, the choice of particular isopycnals enable us to estimate freshwater flux changes on a surface area roughly covering three specific regions of interest: “tropical”, “subtropical” and “subpolar” regions of both south and north hemispheres. In the Atlantic, we bound the isopycnal layer with a maximum of $\gamma = 27.4$ to exclude the influence of the overflows from large marginal seas that are known to have a large impact on the salt budget of the basin and which could affect our salt conservation computations, namely the MOW (with a main core approximately located on $\gamma = 27.5$) and LSW (with a core approximately located on $\gamma = 27.8$). The area delimited by the outcrops of isopycnal $\gamma = 24$ approximately covers the tropical region, the $\gamma = 24$ and $\gamma = 26.5$ outcrops encompass the subtropical gyres in both hemispheres, and the $\gamma = 26.5$ and $\gamma = 27.4$ outcrops encompass large parts of the Southern Ocean and the North Atlantic subpolar gyre. For the Pacific Ocean, tropical, subtropical and subpolar regions are delimited by $\gamma < 23$, $23 \leq \gamma < 25.5$, and $25.5 \leq \gamma < 27.4$, respectively. For the Indian Ocean, tropical, subtropical and subpolar regions are delimited by $\gamma < 23$, $23 \leq \gamma < 26.2$, and $26.2 \leq \gamma < 27.4$, respectively.

Figure 16 shows averaged salinity trends over 1950–2010 in isopycnal layers, with surface outcrops delimiting tropical, subtropical and subpolar regions for each ocean basin, as defined above. In the tropics, the isopycnal layer is bounded by the sea surface and $\gamma = 24$ for the Atlantic, and $\gamma = 23$ for the Pacific/Indian oceans. These isopycnal surfaces lie in the upper thermocline in most parts of the tropical ocean, with surface outcrops

Fig. 16 Salinity linear trend (pss/60 years) over 1950–2010 in isopycnal layers with surface outcrops delimiting “tropical”, “subtropical”, and “subpolar” regions for each ocean basin as defined in the text **a** $\gamma < 23$ (Pacific/Indian) and $\gamma < 24$ (Atlantic). **b** $23 \leq \gamma < 25.5$ (Pacific), $23 \leq \gamma < 26.2$ (Indian), and $24 \leq \gamma < 26.5$ (Atlantic). **c** $25.5 \leq \gamma < 27.4$ (Pacific), $26.2 \leq \gamma < 27.4$ (Indian), and $26.5 \leq \gamma < 27.4$ (Atlantic). Climatological mean isopycnal surface outcrops delimiting each region are also plotted (black solid lines). Areas where the linear trend is not significant at the 95 % confidence level are stippled in gray



encompassing the ITCZ. Spatially coherent broad-scale patterns of salinity change are indicative of the integrated surface freshwater flux change over this period in each

oceanic basin. In the Atlantic, a strong salinity gain is evident throughout this isopycnal volume, indicating an increase in the net evaporation at the sea surface (Fig. 16a).

Similarly in the Indian Ocean, there is net basin-scale salinity gain within this isopycnal volume (although much less so than in the Atlantic), again the result of increased net evaporation at the surface. On the other hand, in the tropical Pacific there is a strong decreasing trend in the western part of the basin, revealing a large freshening of the Western Pacific Warm Pool, while there are no significant trends in most of the central and eastern parts of the basin.

The isopycnal layer with surface outcrops delimiting subtropical regions, encompasses lower thermocline waters in most of the tropical and subtropical areas. In both the Atlantic and Indian oceans, there is a widespread salinity increasing trend throughout this isopycnal volume, indicating a strong increase in net evaporation at the sea surface in the subtropics (Fig. 16b). On the other hand, in the Pacific Ocean, the strong salinity gain across the South Pacific subtropical gyre is largely compensated by a broad-scale freshening trend in the western part of the North Pacific subtropical gyre. The isopycnal layer with surface outcrops delimiting subpolar regions, encompasses intermediate/mode waters throughout the global ocean. A widespread freshening is evidenced throughout this isopycnal volume in the south hemisphere following the pathways of Subantarctic and Subpolar mode waters within all three oceanic basins (Fig. 16c). A broad-scale freshening is also observed in the North Pacific, resulting in a strong net precipitation increase over the whole high-latitude Pacific ocean. In contrast, in the North Atlantic this isopycnal volume exhibits patches of both increasing and decreasing salt content with no evidence of broad-scale pattern of freshwater flux change.

The inferred values of the various area-averaged E–P trends for each oceanic basin and for both 1950–2010 and 1979–2010 periods are shown in Table 1. From the inferred E–P trends we then estimate the corresponding amplification rates of the E–P field for each region (i.e. with respect to the area-averaged E–P climatological annual mean). Area-averaged E–P climatological means are computed here using the hybrid re-analysis/observational OAFflux/GPCP dataset. Differences in estimated area-averaged amplification rates, due to the choice of the E–P dataset, are generally small (i.e. <10 %). The change in the estimated area-averaged amplification rates due to the choice of the isopycnal surfaces is also relatively small and depends on the ratio of surface outcropping area to total volume bounded by the isopycnal surfaces. Hence the change in the amplification rate is lower than 5 %/0.1 kg m⁻³ in the tropical regions, where this ratio is relatively large, while it is around 10 %/0.1 kg m⁻³ in the subpolar regions, where this ratio is much smaller.

In the tropical Atlantic, weak and not statistically significant trends (i.e. at the 95 % confidence interval) are

obtained over both 1950–2010 and 1979–2010 periods, associated with substantial inter-decadal variability of salt content in the respective isopycnal volume. In the Atlantic north/south hemisphere subtropical regions, the inferred E–P change over 1950–2010 is about +0.59 (±0.32) cm/year ($p < 0.05$) whilst it is much stronger over 1979–2010, at 1.61 (±0.75) cm/year ($p < 0.05$). The corresponding amplification rate of the mean E–P field is about 1.3 (±0.7) % and 3.5 (±1.6) % over 1950–2010 and 1979–2010, respectively. In the Atlantic subpolar regions, the inferred E–P change is relatively weak over 1950–2010 [–0.39 (±0.21) cm/year, $p < 0.05$] whilst it is several times stronger over 1979–2010, at –1.81 (±0.53) cm/year ($p < 0.05$). The corresponding amplification rates are about 1.1 (±0.6) % and 5.1 (±1.5) %, respectively.

In the Pacific Ocean tropical region (isopycnal volume bounded by $\gamma = 23$ outcrops) the inferred E–P trends are again weak and not statistically significant over both 1950–2010 and 1979–2010, reflecting again the large intra-decadal and inter-decadal spatiotemporal variability in the tropics that skews long-term trends. In the subtropical regions (isopycnal volume bounded by $\gamma = 23$ and $\gamma = 25.5$ outcrops), a statistically significant positive trend is only obtained for the 1979–2010 period, with the inferred E–P change [$\sim +0.45$ (±0.31) cm/year] implying an amplification rate of about 1.2 (±0.8) %. In the subpolar regions (isopycnal volume bounded by $\gamma = 25.5$ and $\gamma = 27.4$ outcrops), the inferred E–P change is about –2.81 (±1.22) cm/year ($p < 0.05$) over 1950–2010 whilst the freshening is again much stronger over 1979–2010, at –5.91 (±2.16) cm/year ($p < 0.05$). The corresponding amplification rates are about 6.4 (±2.8) % and 13.4 (±4.9) %, respectively.

In the Indian Ocean tropical region (isopycnal volume bounded by $\gamma = 23$ outcrops), similarly to the other two basins, very weak and not statistically significant E–P trends are obtained over both 1950–2010 and 1979–2010. In the subtropical regions (isopycnal volume bounded by $\gamma = 23$ and $\gamma = 26.2$ outcrops), the inferred E–P change is about +0.77 (±0.36) cm/year ($p < 0.05$) over 1950–2010 and +0.59 (±0.35) cm/year ($p < 0.05$) over 1979–2010. The corresponding amplification rates are about 1.3 (±0.6) % and 1 (±0.6) %, respectively. In the subpolar regions (isopycnal volume bounded by $\gamma = 26.2$ and $\gamma = 27.4$ outcrops), the inferred E–P change is about –1.82 (±0.76) cm/year ($p < 0.05$) over 1950–2010 whilst again the freshening is stronger over 1979–2010, at –2.83 (±1.43) cm/year ($p < 0.05$). The corresponding amplification rates are about 3.9 (±1.6) % and 6.1 (±3.1) %, respectively.

At global scale, the increase in net precipitation over subpolar regions is 1.71 (±0.82) cm/year, whereas the increase in net evaporation over the tropical and

Table 1 E–P change (cm/year) inferred from the yearly volume-averaged salinity change in a volume bounded by specific neutral density surfaces for each oceanic basin using salt conservation equation

	Atlantic Ocean		Pacific Ocean		Indian Ocean		
	γ range	E–P change (cm/year)	γ range	E–P change (cm/year)	γ range	E–P change (cm/year)	
		1950–2010	1979–2010	1950–2010	1979–2010	1950–2010	1979–2010
Tropics	<24	+0.29* \pm 0.25	–0.08* \pm 0.16	–0.03* \pm 0.15	+0.29* \pm 0.35	<23	+0.17* \pm 0.24
Subtropics	24–26.5	+0.59 \pm 0.32	+1.61 \pm 0.75	+0.10* \pm 0.22	+0.45 \pm 0.31	23–26.2	+0.77 \pm 0.36
Subpolar	26.5–27.4	–0.39 \pm 0.21	–1.83 \pm 0.53	–2.81 \pm 1.22	–5.91 \pm 2.16	26.2–27.4	–1.82 \pm 0.76

Values of E–P total change are shown for both 1950–2010 and 1979–2010 periods. Error estimates are presented at the 95 % confidence interval

* Not statistically significant trends at the 95 % confidence interval

subtropical regions is 0.43 (\pm 0.28) cm/year, over 1950–2010. In the context of these estimates based on outcropping isopycnal surfaces, tropical/subtropical regions cover an area approximately 3.5 times that of subpolar regions, so these changes are approximately equivalent in magnitude within error estimates—i.e. mass is conserved.

The inferred E–P changes illustrate the contrasting amplification patterns between Atlantic and Pacific subtropical and subpolar regions. The Atlantic (Pacific) ocean basin is characterised by strong water cycle amplification with large positive (negative) E–P trends in the subtropical (subpolar) regions and relatively weak amplification in the subpolar (subtropical) regions. The basin-wide inferred E–P change derived from the salinity change over the isopycnal volume bounded by the $\gamma = 27.4$ outcrops amounts to about +0.25 (\pm 0.22) cm/year for the Atlantic Ocean and –0.70 (\pm 0.29) cm/year for the Pacific Ocean, highlighting the enhancement of salinity/E–P contrast between the two basins. Our results demonstrate that the inferred E–P amplification rates become much higher over 1979–2010 in most of the considered regions. In the global tropical region, inferred E–P trends are weak and not statistically significant, probably reflecting the high spatiotemporal variations associated with natural decadal modes of variability such as ENSO. Again, this underlines the difficulty in separating out the secular changes associated with global-scale warming from the internally generated variability in atmospheric circulation.

At the global scale, inferred E–P changes over 1950–2010 imply a 1 % (\pm 0.6 %) increase in net evaporation over the subtropical regions and a 4.2 % (\pm 2 %) increase in net precipitation over the subpolar regions (Table 2). The global E–P amplification over 1950–2010 is estimated to be about 2.1 (\pm 1.1) %. This is quite small compared to the PA estimate of Durack et al. (2012) over 1950–2000 (\sim 4 %) that is based on the observed SSS and the CMIP3 ensemble E–P/SSS relationship. This may be explained by the large difference in the estimated surface salinity PA among the two studies (i.e. 4.5 vs. 8.0 % for the 1950–2000 nominal period), which is probably attributed to the objective analysis methodology applied in the monthly EN3 dataset and the poor spatiotemporal sampling over the early decades of the observational record, resulting in underestimation of the long-term salinity trends. Interestingly, the ratio between SSS PA (5.3 %) and inferred E–P PA (2.1 %) obtained here over 1950–2010 (\sim 2.5) is close to that derived by the CMIP3 ensemble mean (\sim 2). Our inferred global E–P amplification rate is much lower compared to the E–P PA derived by the re-analysis products above (NCEP/NCAR: 6.5 %, 20CRv2: 7 %). The much larger E–P amplification rate estimates based on the re-analysis products are not surprising since the re-analysis

Table 2 Salinity-inferred regional and global ocean water flux amplification rates for both 1950–2010 and 1979–2010 periods

	Amplification rate (%)	
	1950–2010	1979–2010
Subtropics	1 ± 0.6	2.1 ± 1.1
Subpolar	4.2 ± 2.0	8.5 ± 3.2
Global	2.1 ± 1.1 (4.7 %/°C)	4.1 ± 2.4 (9.8 %/°C)

Error estimates are presented at the 95 % confidence interval. Global ocean water flux amplification sensitivity to warming is also provided in parentheses

models have been shown to produce too-intense water cycling, overestimating both P and E (e.g. Trenberth et al. 2011).

Inferred E–P changes over 1979–2010 imply ~ 2 (± 1.1) % increase in net evaporation over the subtropical regions and 8.5 (± 3.2) % increase in net precipitation over the subpolar regions. The inferred global E–P amplification rate is much higher over 1979–2010 reaching 4.1 (± 2.4) %, which is comparable to the estimate of Hosoda et al. (2009) (~ 3.7 % over 1974–2005), also inferred from observed salinity changes. Our inferred E–P changes over the subpolar regions are lower than those inferred by Helm et al. (2010) over the 1970–2005 period. This is expected, as our inferred estimate is closer to a pure local freshwater flux change as opposed to that of Helm et al. (2010), where the sub-surface salinity change pattern used to infer the E–P change may be attributed to both local surface freshwater flux changes and to changes associated to a predominantly poleward shift of the isopycnal outcropping locations due to warming. The discrepancy is much higher in the Southern Ocean, where Helm et al. infer a very large amplification rate, namely an increase in net precipitation of 16 % over 1970–2005. Consistent with this, Durack and Wijffels (2010) showed that the major contributor to the sub-surface salinity decrease in the southern hemisphere sub-tropics was the poleward migration of isopycnal outcropping surfaces in the Southern Ocean.

Inferred global E–P changes over 1950–2010 and 1979–2010 were also assessed alongside estimates of coincident global sea surface temperature change (Table 2), which is considered to be the natural thermodynamic framework of water cycle amplification (Durack et al. 2012). The Clausius–Clapeyron (CC) relationship indicates a ~ 7 % increase in low-level atmospheric moisture per degree of warming, assuming constant relative humidity. Following Held and Soden (2006), the E–P pattern must also satisfy this CC scaling in the hypothesis that the large-scale atmospheric circulation has been stable. Based on the inferred global amplification rate of 2.1 % and the SST change deduced from the HadSST3 dataset

over 1950–2010, we deduce a water flux amplification sensitivity of about $4.7 \text{ \% } ^\circ\text{C}^{-1}$ which is well below the CC rate ($\sim 7 \text{ \% } ^\circ\text{C}^{-1}$). This is also much lower than that estimated by Durack et al. (2012) over 1950–2000 ($\sim 8 \text{ \% } ^\circ\text{C}^{-1}$), which is again expected given the much larger surface salinity PA obtained in the latter study. However, our inferred global E–P amplification rate is almost two times higher over 1979–2010 (4.1 %), which is consistent with an intensification of the water cycle driven by the accelerated broad-scale warming over this period. On the other hand, Durack et al. (2012) also performed their salinity trend analysis over 1975–2008 and found the resulting trends to be only slightly larger than for the full 1950–2008 analysis, with similar though not identical spatial patterns. The large increase in the inferred amplification rate obtained here could be a consequence of much improved salinity sampling over the latter period, particularly in the southern hemisphere, which, in turn, resulted in a proper representation of salinity anomalies by the objective analysis. Considering the 1979–2010 changes, the deduced water flux amplification sensitivity is about $9.8 \text{ \% } ^\circ\text{C}^{-1}$, now above the CC rate. However, as shown in the previous section, water cycle changes over this shorter period are also partially driven by decadal scale natural modes of variability such as ENSO and/or changes in the atmospheric tropical circulation (Sohn et al. 2013; L’Heureux et al. 2013).

4 Conclusions

The pattern of multi-decadal salinity change over 1950–2010 obtained here using the EN3 observational dataset supports the results of previous studies (Boyer et al. 2005; Hosoda et al. 2009; Durack and Wijffels 2010; Helm et al. 2010; Durack et al. 2012), revealing an amplification of the mean surface salinity field with salinity increases (decreases) found in most of the evaporation- (precipitation-) dominated regions, consistent with an intensification of the global water cycle. The average global amplification of the surface salinity pattern amounts to 5.3 % over 1950–2010 and agrees well with the previous analyses of Boyer et al. (2005) and Hosoda et al. (2009), however is considerably less than the estimates of Durack and Wijffels (2010) and Helm et al. (2010). The sub-surface salinity change patterns provide further indications of an intensified water cycle, including an accentuation of the upper layer salinity contrast between Atlantic and Pacific oceans as well as between the upper thermocline salinity maximum and the lower thermocline salinity minimum.

Trends in reanalysis-derived E–P over the same 60-year period 1950–2010 have been investigated using the only two reanalysis products that cover this period: NCEP/

NCAR and 20CRv2. The E–P trends are found to be less spatially coherent than for surface salinity. Large differences in the E–P trend patterns between the two products are evident in a number of regions, particularly the North Atlantic. This is of particular concern, given the use of NCEP NWP models for each product, and suggests low confidence in the trends at 60-year timescales. Some improvement in the reliability of the datasets might be expected in the satellite era from 1979 onwards, and we have considered a further four products in this period: COREv2, ERA-Interim, NCEP/DOE and OAFflux-GPCP. However we also note that inhomogeneities between these products are apparent prior to 1987 (Schanze et al. 2010), which further compromise trend estimates. Our results show that there is still a large spread between the different E–P products as regards magnitude and sign of the trends. Results demonstrate the strong limitations and large discrepancies among the re-analysis products in representing long-term variability and trends over the ocean, in agreement with previous studies (Trenberth et al. 2005, 2011; Trenberth and Smith 2005; Schanze et al. 2010). However, a robust pattern of increased E–P in the southern hemisphere subtropical Pacific is seen in all of the products considered.

Some evidence is found for a significant link between surface salinity and E–P change patterns over 1979–2010, based on the blended re-analysis/satellite-derived datasets i.e. mainly OAFflux-GPCP and to a lesser extent COREv2. On the other hand, there is no immediately evident relationship between SSS and E–P change in any of the re-analysis datasets investigated for the two periods considered. The most enhanced and spatially coherent inter-annual correlation patterns over 1979–2010 among all products are obtained between GPCP precipitation and surface salinity. ENSO multi-decadal variability has been shown to exert a significant control on the spatial patterns of E–P/SSS linear trends in the tropical Pacific Ocean over 1979–2010.

Re-analysis products also indicate an amplification of the global E–P pattern. However, the correlation coefficients between the change in E–P and the mean E–P field are in each case very low. Thus, we have been unable to obtain clear evidence for an intensification of the global ocean water cycle using this direct approach. In an alternative approach, we have inferred the amplification rate of the water cycle over specific regions of the global ocean from the observed 3-D salinity change field using a salt conservation equation in variable isopycnal volumes, allowing for isopycnal surface vertical/horizontal migrations. At global scale, inferred E–P changes imply a $\sim 1\%$ increase in net evaporation over the subtropical regions and a $\sim 4.2\%$ increase in net precipitation over the subpolar regions over 1950–2010, while the

amplification rates are approximately doubled over 1979–2010, consistent with accelerated broad-scale warming over this period. However, the large increase in the amplification rate is partially explained by multi-decadal variations in ENSO that impact more strongly over the shorter time-period. On the other hand, this is also coincident with much improved salinity sampling over the latter period, particularly in the southern hemisphere, which probably improves the performance of objective analysis in producing trend estimates.

As a strong caveat, we stress the limits to which objectively-analysed salinity fields can adequately represent the variability and trends in deep layers and in large oceanic regions of the southern hemisphere, which were very poorly sampled prior to the 1970s in particular. Nevertheless, while large discrepancies are found between E–P multi-decadal trend patterns in the various reanalysis/observational global datasets (even over the well-sampled satellite era), a more robust and spatially coherent structure of multi-decadal change is obtained for the salinity field. Importantly, our results are consistent with many other recent studies of multi-decadal salinity change, using different methods and assumptions in their trend analysis, all suggesting a global water cycle amplification induced by broad-scale warming.

One of the key challenging issues regarding the changing water cycle is how to separate out natural low-frequency modes of large-scale variability signals from the long-term trends, and hence to properly attribute water cycle/salinity changes to natural variability or anthropogenic forcing. The signal of ENSO in particular is imprinted in both salinity and E–P change spatial patterns over 1979–2010 and may skew possible anthropogenic long-term climatic trends. The analysis of new high spatiotemporal resolution satellite-derived observations of salinity (e.g. SMOS, Aquarius) and precipitation (e.g. TRMM) along with the continuous acquisition of 3-D salinity data by the ARGO network (achieving an unprecedented near-global ocean observation) will help us to progressively enhance the present knowledge of changing salinity and freshwater fluxes in the World Ocean and to assess the key processes that shape these changes in response to both natural modes of variability and anthropogenic forcing. Moreover, new-generation higher-resolution climate model simulations such as those of the Coupled Model Intercomparison Project phase 5 (CMIP5) database can help us to properly assess the advective pathways of salinity anomalies into the ocean interior and to partition surface forcing of salinity trends between changes in E–P and shifting ventilation sites, both attributable, to different degrees, to anthropogenic and natural causes. Further assessment of the 3-D pattern of salinity change, and of the key processes involved, is expected to

result in more confident projections of the changing water cycle on decadal and global to regional scales.

Acknowledgments This study was part of the “Hydrological Cycle Understanding via Process-based Global Detection, Attribution and Prediction (Horyuji PAGODA)”, supported by the UK Natural Environment Research Council as part of the “Changing Water Cycle” programme (Grant No. NE/I006222/1). Simon Good was supported by the Joint DECC and Defra Integrated Climate Programme, DECC/Defra (GA01101). We are grateful to two anonymous referees for their extremely thorough and constructive reviews.

References

- Adler RF, Huffman GJ, Chang A, Ferraro R, Xie P, Janowiak J, Rudolf B, Schneider U, Curtis S, Bolvin D, Bolvin D, Gruber A, Susskind J, Arkin P, Nelkin EJ (2003) The version 2.1 global precipitation climatology project (GPCP) monthly precipitation analysis (1979—present). *J Hydrometeorol* 4(6):1147–1167
- Allan RP, Soden BJ, John VO, Ingram W, Good P (2010) Current changes in tropical precipitation. *Environ Res Lett* 5:025205. doi:10.1088/1748-9326/5/2/025205
- Alory GSW, Wijffels S, Meyers G (2007) Observed temperature trends in the Indian Ocean over 1960–1999 and associated mechanism. *Geophys Res Lett* 34:L02606. doi:10.1029/2006GL028044
- Andersson A, Klepp C, Fennig K, Bakan S, Hartmut Grassl H, Jörg Schulz J (2011) Evaluation of HOAPS-3 ocean surface freshwater flux components. *J Appl Meteor Climatol* 50:379–398
- Antonov JI, Levitus S, Boyer T (2002) Steric sea level variations during 1957–1994: importance of salinity. *J Geophys Res* 107(C12):8013. doi:10.1029/2001JC000964
- Arkin PA, Smith TM, Sapiano MRP, Janowiak J (2010) The observed sensitivity of the global hydrological cycle to changes in surface temperature. *Environ Res Lett* 5:035201. doi:10.1088/1748-9326/5/3/035201
- Belkin IM (2004) Propagation of the “great salinity anomaly” of the 1990s around the northern North Atlantic. *Geophys Res Lett* 31:L08306. doi:10.1029/2003GL019334
- Belkin IM, Levitus S, Antonov J, Malmberg SA (1998) “Great Salinity Anomalies” in the North Atlantic. *Prog Oceanogr* 41:1–68. doi:10.1016/S0079-6611(98)00015-9
- Bethoux JP, Gentili B (1999) Functioning of the Mediterranean Sea: past and present changes related to freshwater input and climate changes. *J Mar Syst* 20:33–47
- Bindoff NL, McDougall TJ (1994) Diagnosing climate change and ocean ventilation using hydrographic data. *J Phys Oceanogr* 24:1137–1152
- Bindoff NL, Willebrand J, Artale V et al (2007) Observations: oceanic climate change and sea level. In: Solomon S et al (eds) *Climate change 2007: the physical science basis. Contribution of the working group I to the fourth assessment report of the intergovernmental panel on climate change*. Cambridge University Press, Cambridge, pp 385–432
- Boyer TP, Levitus S, Antonov JI, Locarnini RA, Garcia HE (2005) Linear trends in salinity for the World Ocean, 1955–1998. *Geophys Res Lett* 32:L01604. doi:10.1029/2004GL021791
- Boyer TP, Levitus S, Antonov JI, Locarnini RA, Mishonov A, Garcia HE, Josey SA (2007) Changes in freshwater content in the North Atlantic Ocean 1955–2006. *Geophys Res Lett* 34:L16603. doi:10.1029/2007GL030126
- Chou C, Neelin JD, Chen C-A, Tu J-Y (2009) Evaluating the “rich get richer” mechanism in tropical precipitation change under global warming. *J Clim* 22:1982–2005
- Compo GP, Whitaker JS, Sardeshmukh PD et al (2011) The twentieth century reanalysis project. *Q R Meteorol Soc* 137:1–28. doi:10.1002/qj.776
- Cravatte S, Delcroix T, Zhang D, McPhaden M, LeLoup J (2009) Observed freshening and warming of the western Pacific Warm Pool. *Clim Dyn* 33:565–589. doi:10.1007/s00382-009-0526-7
- Curry R, Mauritzen C (2005) Dilution of the northern North Atlantic Ocean in recent decades. *Science* 308:1772–1774. doi:10.1126/science.1109477
- Curry RG, McCartney MS (2001) Ocean gyre circulation changes associated with the North Atlantic Oscillation. *J Phys Oceanogr* 31:3374–3400. doi:10.1175/1520-0485(2001)031<3374:OGC CAW>2.0.CO;2
- Curry R, Dickson B, Yashayaev I (2003) A change in the freshwater balance of the Atlantic Ocean over the past four decades. *Nature* 426:826–829. doi:10.1038/nature02206
- Dee DP, Uppala SM, Simmons AJ et al (2011) The ERA-Interim reanalysis: configuration and performance of the data assimilation system. *Q J R Meteorol Soc* 137:553–597. doi:10.1002/qj.828
- Delcroix T, Alory G, Cravatte S, Corrège T, McPhaden M (2011) A gridded sea surface salinity data set for the tropical Pacific with sample applications (1950–2008). *Deep Sea Res* 58:38–48. doi:10.1016/j.dsr.2010.11.002
- Dickson RR, Meincke J, Malmberg S, Lee AJ (1988) The “great salinity anomaly” in the northern North Atlantic 1968–1982. *Prog Oceanogr* 20:103–151
- Durack PJ, Wijffels SE (2010) Fifty-year trends in global ocean salinities and their relationship to broad-scale warming. *J Clim* 23:4342–4362. doi:10.1175/2010JCLI3377.1
- Durack PJ, Wijffels SE, Matear RJ (2012) Ocean salinities reveal strong global water cycle intensification during 1950 to 2000. *Science* 336:455–458. doi:10.1126/science.1212222
- Gille ST (2002) Warming of the Southern Ocean since the 1950s. *Science* 295(5558):1275–1277. doi:10.1126/science.1065863
- Gille ST (2008) Decadal-scale temperature trends in the southern hemisphere ocean. *J Clim* 21(18):4749–4765. doi:10.1175/2008JCLI2131.1
- Gouretski V, Koltermann KP (2007) How much is the ocean really warming? *Geophys Res Lett* 34(1):L01610. doi:10.1029/2006GL027834
- Hasson AEA, Delcroix T, Dussin R (2013) An assessment of the mixed layer salinity budget in the tropical Pacific Ocean. Observations and modelling (1990–2009). *Ocean Dyn* 63(2–3):179–194. doi:10.1007/s10236-013-0596-2
- Held IM, Soden BJ (2006) Robust responses of the hydrological cycle to global warming. *J Clim* 19:5686–5699. doi:10.1175/JCLI3990.1
- Helm KP, Bindoff NL, Church JA (2010) Changes in the global hydrological-cycle inferred from ocean salinity. *Geophys Res Lett* 37:L18701. doi:10.1029/2010GL044222
- Hosoda S, Suga T, Shikama N, Mizuno K (2009) Global surface layer salinity change detected by Argo and its implication for hydrological cycle intensification. *J Oceanogr* 65:579–586. doi:10.1007/s10872-009-0049-1
- Huffman GJ, Adler RF, Bolvin DT, Gu G (2009) Improving the global precipitation record: GPCP version 2.1. *Geophys Res Lett* 36:L17808. doi:10.1029/2009GL040000
- Hurrell JW (1995) Decadal trends in the North Atlantic Oscillation: regional temperatures and precipitation. *Science* 269:676–679. doi:10.1126/science.269.5224.676

- Hurrell JW, Deser C (2010) North Atlantic climate variability: the role of the North Atlantic Oscillation. *J Mar Syst* 79:231–244. doi:[10.1016/j.jmarsys.2009.11.002](https://doi.org/10.1016/j.jmarsys.2009.11.002)
- Ingleby B, Huddleston M (2007) Quality control of ocean temperature and salinity profiles-historical and real-time data. *J Mar Syst* 65:158–175. doi:[10.1016/j.jmarsys.2005.11.019](https://doi.org/10.1016/j.jmarsys.2005.11.019)
- John VO, Allan RP, Soden BJ (2009) How robust are observed and simulated precipitation responses to Tropical Ocean warming? *Geophys Res Lett* 36:L14702
- Kanamitsu M, Ebisuzaki W, Woollen J, Yang S, Hnilo J, Fiorino M, Potter G (2002) NCEP DOE AMIP-II reanalysis (r-2). *Bull Am Meteorol Soc* 83:1631–1643
- Kavvada A, Ruiz-Barradas A, Nigam S (2013) AMO's structure and climate footprint in observations and IPCC AR5 climate simulations. *Clim Dyn*. doi:[10.1007/s00382-013-1712-1](https://doi.org/10.1007/s00382-013-1712-1)
- Kistler R, Kalnay E, Collins W, Saha S, White G, Woollen J, Chelliah M, Ebisuzaki W, Kanamitsu M, Kousky V et al (2001) The NCEP–NCAR 50-year reanalysis: monthly means CD-ROM and documentation *Bull. Bull Am Meteorol Soc* 82:247–267
- L'Heureux ML, Lee S, Lyon B (2013) Recent multidecadal strengthening of the Walker circulation across the tropical Pacific. *Nat Clim Change* 3:571–576. doi:[10.1038/NCLIMATE1840](https://doi.org/10.1038/NCLIMATE1840)
- Large W, Yeager S (2009) The global climatology of an interannually varying air–sea flux dataset. *Clim Dyn* 33:341–364
- Lau K-M, Wu H-T (2007) Detecting trends in tropical rainfall characteristics, 1979–2003. *Int J Climatol* 27:979–988. doi:[10.1002/joc.1454](https://doi.org/10.1002/joc.1454)
- Li L, Jiang X, Chahine MT, Olsen ET, Fetzer EJ, Chen L, Yung YL (2011) The recycling rate of atmospheric moisture over the past two decades (1988–2009). *Env Res Lett* 6:034018. doi:[10.1088/1748-9326/6/3/034018](https://doi.org/10.1088/1748-9326/6/3/034018)
- Liu C, Allan RP (2012) Multi-satellite observed responses of precipitation and its extremes to interannual climate variability. *J Geophys Res* 117:D03101. doi:[10.1029/2011JD016568](https://doi.org/10.1029/2011JD016568)
- Liu J, Xiao T, Chen L (2011) Intercomparisons of air–sea heat fluxes over the Southern Ocean. *J Clim* 24(4):1198–1211. doi:[10.1175/2010JCLI3699.1](https://doi.org/10.1175/2010JCLI3699.1)
- Liu C, Allan RP, Huffman GJ (2012) Co-variation of temperature and precipitation in CMIP5 models and satellite observations. *Geophys Res Lett* 39:L13803. doi:[10.1029/2012GL052093](https://doi.org/10.1029/2012GL052093)
- Lozier MS, Stewart NM (2008) On the temporally northward penetration of Mediterranean overflow water and eastward penetration of Labrador Sea Water. *J Phys Oceanogr* 38:2097–2103
- McCartney MS, Mauritzen C (2001) On the origin of the warm inflow to the Nordic Seas. *Prog Oceanogr* 51:125–214
- Meehl GA, Stocker TF, Collins WD et al (2007) Global climate projections. In: Solomon S et al (eds) *Climate change 2007: the physical science basis, contribution of working group 1 to the fourth assessment report of the intergovernmental panel on climate change*. Cambridge University Press, New York, pp 747–845
- Merrifield MA (2011) A shift in Western Tropical Pacific sea level trends during the 1990s. *J Clim* 24:4126–4138. doi:[10.1175/2011JCLI3932.1](https://doi.org/10.1175/2011JCLI3932.1)
- Pierce DW, Gleckler PJ, Barnett TP, Santer BD, Durack PJ (2012) The fingerprint of human-induced changes in the ocean's salinity and temperature fields. *Geophys Res Lett* 39:L21704. doi:[10.1029/2012GL053389](https://doi.org/10.1029/2012GL053389)
- Potter R, Lozier S (2004) On the warming and salinification of the Mediterranean outflow waters in the North Atlantic. *Geophys Res Lett* 31:L01202. doi:[10.1029/2003GL018161](https://doi.org/10.1029/2003GL018161)
- Reid JL (1979) On the contribution of the Mediterranean Sea outflow to the Norwegian–Greenland Sea. *Deep Sea Res Part A* 26:1199–1223
- Richter I, Xie SP (2010) Moisture transport from the Atlantic to the Pacific basin and its response to North Atlantic cooling and global warming. *Clim Dyn* 35:551–566
- Rixen M et al (2005) The Western Mediterranean deep water: a proxy for climate change. *Geophys Res Lett* 32:L12608. doi:[10.1029/2005GL022702](https://doi.org/10.1029/2005GL022702)
- Rohling EJ, Bryden HL (1992) Man-induced salinity and temperature increases in western Mediterranean water. *J Geophys Res* 97:11191–11198
- Santer BD, Mears C, Wentz FJ et al (2007) Identification of human-induced changes in atmospheric moisture content. *Proc Nat Acad Sci* 104(39):15248–15253
- Schanze JJ, Schmitt RW, Yu LL (2010) The global oceanic freshwater cycle: a state-of-the-art quantification. *J Mar Res* 68:569–595. doi:[10.1357/002224010794657164](https://doi.org/10.1357/002224010794657164)
- Schmitt RW (2008) Salinity and the global water cycle. *Oceanography* 21:12–19. doi:[10.5670/oceanog.2008.63](https://doi.org/10.5670/oceanog.2008.63)
- Skirris N, Sofianos S, Lascaratos A (2007) Hydrological changes in the Mediterranean Sea in relation to changes in the freshwater budget: a numerical modelling study. *J Mar Syst* 65:400–416
- Sohn BJ, Yeh SW, Schmetz J, Song HJ (2013) Observational evidences of Walker circulation change over the last 30 years contrasting with GCM results. *Clim Dyn* 40:1721–1732. doi:[10.1007/s00382-012-1484-z](https://doi.org/10.1007/s00382-012-1484-z)
- Solomon S, Qin D, Manning M, Marquis M, Averyt KB, Tignor MM, Miller HL Jr, Chen Z (eds) (2007) *Climate change 2007: the physical science basis*. Cambridge University Press, Cambridge
- Stott PA, Sutton RT, Smith DM (2008) Detection and attribution of Atlantic salinity changes. *Geophys Res Lett* 35:L21702. doi:[10.1029/2008GL035874](https://doi.org/10.1029/2008GL035874)
- Sutton R, Hodson D (2003) Influence of the ocean on North Atlantic climate variability 1871–1999. *J Clim* 16:3296–3313. doi:[10.1126/science.1109496](https://doi.org/10.1126/science.1109496)
- Terray L, Corre L, Cravatte S, Delcroix T, Reverdin G, Ribes A (2012) Near-surface salinity as nature's rain gauge to detect human influence on the tropical water cycle. *J Clim* 25:958–977
- Tian Y, Peters-Lidard CD, Eylander JN, Joyce RJ, Huffman GJ, Adler RF, Hsu K-L, Turk FJ, Garcia M, Zeng J (2009) Component analysis of errors in satellite-based precipitation estimates. *J Geophys Res* 114:D24101. doi:[10.1029/2009JD011949](https://doi.org/10.1029/2009JD011949)
- Trenberth KE, Smith L (2005) The mass of the atmosphere: a constraint on global analyses. *J Clim* 18(6):864–875. doi:[10.1175/JCLI-3299.1](https://doi.org/10.1175/JCLI-3299.1)
- Trenberth KE, Fasullo J, Smith L (2005) Trends and variability in column-integrated atmospheric water vapor. *Clim Dyn* 24:741–758. doi:[10.1007/s00382-005-0017-4](https://doi.org/10.1007/s00382-005-0017-4)
- Trenberth KE, Smith L, Qian T, Dai A, Fasullo J (2007) Estimates of the global water budget and its annual cycle using observational and model data. *J Hydrometeorol* 8:758–769. doi:[10.1175/JHM600.1](https://doi.org/10.1175/JHM600.1)
- Trenberth KE, Fasullo J, Mackaro J (2011) Atmospheric moisture transports from ocean to land and global energy flows in reanalyses. *J Clim* 24(18):4907–4924. doi:[10.1175/2011JCLI4171.1](https://doi.org/10.1175/2011JCLI4171.1)
- Tzortzi E, Josey SA, Srokosz M, Gommenginger C (2013) Tropical Atlantic salinity variability: new insights from SMOS. *Geophys Res Lett* 40:2143–2147. doi:[10.1002/grl.50225](https://doi.org/10.1002/grl.50225)
- Vinogradova NT, Ponte RM (2013) Clarifying the link between surface salinity and freshwater fluxes on monthly to inter-annual timescales. *J Geophys Res* 118:3190–3201. doi:[10.1002/jgrc.20200](https://doi.org/10.1002/jgrc.20200)
- Wadley MR, Bigg GR (2006) Are “great salinity anomalies” advective? *J Clim* 19:1080–1088. doi:[10.1175/JCLI3647.1](https://doi.org/10.1175/JCLI3647.1)
- Wentz FJ, Ricciardulli L, Hilburn K, Mears C (2007) How much more rain will global warming bring? *Science* 317(5835):233–235. doi:[10.1126/science.1140746](https://doi.org/10.1126/science.1140746)

- Wijffels S (2001) Ocean transport of fresh water. In: Siedler G, Church J, Gould J (eds) *Ocean circulation and climate*. Academic Press, New York, pp 475–488
- Willett KW, Gillett NP, Jones PD, Thorne PW (2007) Attribution of observed humidity changes to human influence. *Nature* 449:710–712
- Xie P, Arkin PA (1996) Global precipitation: a 17-year monthly analysis based on gauge observations, satellite estimates, and numerical model outputs. *Bull Am Meteorol Soc* 78:2539–2558
- Yin X, Gruber A, Arkin P (2004) Comparison of the GPCP and CMAP Merged Gauge–Satellite monthly precipitation products for the period 1979–2001. *J Hydrometeorol* 5:1207–1222. doi:[10.1175/JHM-392.1](https://doi.org/10.1175/JHM-392.1)
- Yu L (2011) A global relationship between the ocean water cycle and near-surface salinity. *J Geophys Res* 116:C10025. doi:[10.1029/2010JC006937](https://doi.org/10.1029/2010JC006937)
- Yu L, Weller RA (2007) Objectively analyzed air–sea flux fields for the global ice-free oceans (1981–2005). *Bull Am Meteorol Soc* 88:527–539
- Yu L, Jin X, Weller RA (2008) Multidecade global flux datasets from the Objectively Analyzed air–sea Fluxes (OAFflux) project: latent and sensible heat fluxes, ocean evaporation, and related surface meteorological variables. OAFflux project technical report (OA2008–01), Woods Hole Oceanographic Institution
- Zhang et al (2007) Detection of human influence on twentieth-century precipitation trends. *Nature* 448:461–465. doi:[10.1038/nature06025](https://doi.org/10.1038/nature06025)